DEVELOPMENT OF A MICROENGINEERED HUMAN BLOOD-BRAIN BARRIER MODEL WITH 3D ASTROCYTIC NETWORK

A Dissertation
Presented to
The Academic Faculty

by

Song Ih Ahn

In Partial Fulfillment
of the Requirements for the Degree
Doctor of Philosophy in the
Bioengineering

Georgia Institute of Technology
December 2019

DEVELOPMENT OF A MICROENGINEERED HUMAN BLOOD-BRAIN BARRIER MODEL WITH 3D ASTROCYTIC NETWORK

Approved by:

Dr. YongTae Kim, Advisor
George W. Woodruff School of Mechanical Engineering
Georgia Institute of Technology

Dr. Shuichi Takayama
Wallace H. Coulter Department of Biomedical Engineering
Georgia Institute of Technology

Dr. Allan I. Levey
Department of Neurology
Emory University

Dr. Levi Wood
George W. Woodruff School of Mechanical Engineering
Georgia Institute of Technology

Dr. Mark R. Prausnitz
School of Chemical & Biomolecular Engineering
Georgia Institute of Technology

Date Approved: September 03, 2019

To my family

ACKNOWLEDGEMENTS

First of all, I would like to thank my advisor, Dr. YongTae Kim, for his mentoring and support during my journey as a Ph.D. student. His invaluable advice has helped me in pursuing my career goal as a researcher. I also wish to thank my committee members, Dr. Allan Levey, Dr. Mark Prausnitz, Dr. Shuichi Takayama, and Dr. Levy Wood for their personal and professional guidance and insightful comments on my research. I would like to express my appreciation to Dr. Jennifer Shin, who always supports and encourages me.

I am also grateful to my past and current lab members. I would especially like to thank Dr. Yoshitaka Sei, Dr. Candice Hovell, and Angel Santiago-Lopez. I could not have imagined having better lab mates and friends like you. I would like to extend my sincere thanks to Dr. Hyun-Ji Park, Dr. Jinhwan Kim, Jiwon Yom, and Yujung Ryu for their help and dedication to my research.

I would like to extend my greatest gratitude to my friends. My time at Georgia Tech will remain happy memory because of you.

Last but not least, my deepest appreciation goes to my family. Thank you to my Mom, Dad, and my sister for their warm love and endless support. I would like to express my heartfelt appreciation and love to my husband, Hyunggwi Song. My Ph.D. journey would not have been possible without your love and support.

TABLE OF CONTENTS

LIST OF TABLES

LIST OF FIGURES

LIST OF SYMBOLS AND ABBREVIATIONS

2D	Two-dimensional
3D	Three-dimensional
A	Astrocyte medium
AQP4	Aquaporin-4
Aβ	Amyloid beta
BBB	Blood-brain barrier
BLT-1	Block lipid transport-1
CERP	Cholesterol efflux regulatory protein
CLDN5	Claudin-5
CNS	Central nervous system
DALYs	Disability-adjusted life years
E	Endothelial cell medium
ECM	Extracellular matrix
eHNP-A1	Engineered HDL-mimetic nanoparticle with apolipoprotein A1
FACS	Fluorescence-activated cell sorting
G	Glia medium
GAPDH	Glyceraldehyde 3-phosphate dehydrogenase
GFAP	Glial fibrillary acidic protein
GLUT1	Glucose transporter 1
HA	Human astrocyte
HBMEC	Human brain microvascular endothelial cell
HBVP	Human brain vascular pericyte

HDL	High-density lipoprotein
HUVEC	Human umbilical vascular endothelial cell
IF	Intermediate filaments
IL-1β	Interlukin-1β
iPSC	Induced pluripotent stem cell
LCN2	Lipocalin-2
LDLR	Low-density lipoprotein receptor
LRP1	Low-density lipoprotein receptor related protein 1
M	Microglia medium
NP	Nanoparticle
OCLN	Occludin
P	Pericyte medium
PDMS	Polydimethylsiloxane
P-gp	P-glycoprotein
Serpina3n	Serpin Family A Member 3
SR-B1	Scavenger receptor type B1
TEER	Transendothelial electrical resistance
VE-cad	Vascular endothelial cadherin
VIM	Vimentin
ZO-1	Zonula occluden-1

SUMMARY

The blood-brain barrier (BBB), a unique vascular border in the central nervous system (CNS), has a highly selective barrier function that prevents unwanted substances from entering the brain. To deliver drugs into the brain, CNS delivery systems have been widely explored to cross the BBB. However, the lack of experimental models that can precisely analyze the interactions between the BBB and delivery platforms restricts successful clinical translation of CNS therapeutics. Despite valuable contribution of animal models to drug discovery, it remains difficult to conduct mechanistic studies on the barrier function and interactions with drugs at molecular and cellular levels. One innovative approach to addressing this challenge is to develop an *in vitro* model that mimics the essential physiological structure and function of the human BBB and that allows quantitative analysis of drug transport across the barrier in a controlled manner. The main focus of this thesis is on development of a microengineered human BBB model which reconstitutes the key structure and function of the human BBB and enables 3D capturing of nanoparticle distribution at tissue and cellular levels to demonstrate the mechanisms of cellular uptakes and BBB penetration. This BBB model may present a complementary *in vitro* model to animal models for prescreening drug candidates for the treatment of CNS diseases.

CHAPTER 1. INTRODUCTION

1.1 Background

1.1.1 High failure rate of the central nervous system (CNS) drug development

Neurological disorders including neurodegenerative diseases, cerebrovascular diseases, and brain tumors are the second leading cause of death worldwide. Moreover, the number of people affected by neurological disorders has been increasing worldwide, with approximately a 15% increase of disability-adjusted life years (DALYs) since 1990.[1] However, the success rate in clinical trials for the drugs targeting neurological diseases remains 8.4%, which is low compared to the success rates for other drugs.[2] This challenge is mainly due to a unique central nervous system (CNS) barrier structure, the blood-brain barrier (BBB).[1]

1.1.2 Blood-brain barrier (BBB)

The BBB is a highly functionalized vascular barrier of the CNS that controls the transport of substances between the blood and brain.[3] The selective permeability of the BBB remains as the major challenge in development of CNS therapeutics, and at the same time, many CNS diseases are associated with BBB breakdown that can lead to uncontrolled entry of pathogens and immune cells into the brain.[4] Therefore, understanding the complex physiology of the BBB and transport mechanisms in both physiological and pathological conditions is critical to study pathophysiology of the CNS diseases as well as to develop CNS therapeutics.

The BBB consists of the specialized microvascular endothelium with surrounding basement membrane, pericytes, and astrocytes (Figure 1.1), and these constituent cells of the BBB contributes to the BBB integrity and the selective barrier function.[5,6] A major component of the BBB is the brain endothelial cells lining the blood vessels in the brain that are highly specialized compared to the endothelial cells in other organs. These brain endothelial cells are characterized with particularly strong expression of tight junctions (e.g. zonula occluden-1 (ZO-1), occludin (OCLN), and claudin-5 (CLDN5)), BBB-specific membrane transporters (e.g. glucose transporter 1 (GLUT1) and p-glycoprotein (P-gp)) and receptors (e.g. low-density lipoprotein receptor related protein 1 (LRP1)).[7-9] Moreover, the apical surface membrane of the brain endothelial cells are exposed to a continuous blood flow with shear stress in a range between 4~20 dyne/cm^2. Pericytes embedded in the basement membrane wrap around the endothelium and contribute to astrocytic polarization and microvascular stability.[10] The density of pericytes along the blood vessel is high in the brain with the ratio between 1:1 and 1:3 (pericytes : endothelial cells),[3] while the ratio in skeletal muscle is known to be close to 1:10.[11] Although the role of pericytes in BBB function has not been studied much compared to other constituent cells, recent studies have demonstrated their critical roles in the formation and regulation of the BBB, and the integration of endothelial and astrocyte functions.[10,12] Astrocytes form the glia limitans of the BBB with their end-feet contacting the blood vessels and control the influx of water through aquaporin-4 (AQP4).[13,14] These astrocytes construct a three-dimensional (3D) network with their typical star-like shapes and long branches in radial distribution along their cell bodies.[15] The function of perivascular astrocytes at the BBB in physiological and pathological conditions will be further discussed in the next section.

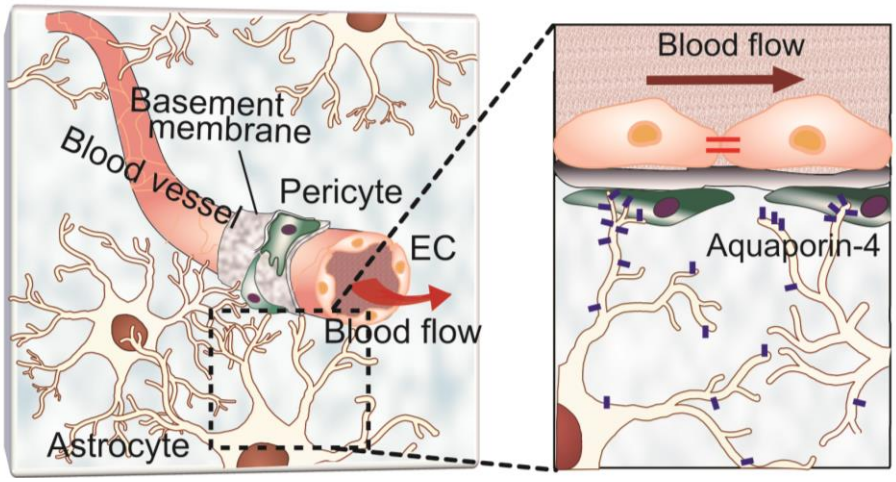

Figure 1.1 Structure of the blood-brain barrier. The BBB is consisting of blood vessel aligned with brain endothelial cells, basement membrane, pericytes, and astrocytes that covers the blood vessel. Endothelial cells at the blood vessel are exposed to a continuous blood flow and astrocytic end-feet near the blood vessel show polarized expression of aquaporin-4.

1.1.3 Physiology of astrocytes at the BBB

Astrocytes are highly heterogeneous cells with different functions and morphologies, and these cells change their phenotype in response to CNS injuries and diseases.[16] In the healthy brain, astrocytes show long branched processes around their cell bodies.[15] These astrocytes cover ~99% of the perivascular surface of the brain microvessels with their end-feet and secrete factors that control formation, maintenance, and function of the BBB.[16] Under CNS pathological conditions, astrocytes become reactive and contribute to disease progression which may lead to BBB breakdown and disease progression such as neurodegeneration, ischemia, and infection.[15,17,18] These reactive astrocytes undergo changes in morphology and gene expressions. Upregulation of astrocyte intermediate filaments (IFs) such as glial fibrillary acidic protein (GFAP) and vimentin (VIM) have been used as the most common hallmark of reactive astrocytes. However, IFs were not strong

markers to identify reactive astrocytes as the expression level of the IFs in astrocytes varies with the developmental stage and the IFs are widely expressed in most astrocytes even in non-reactive states. Recently, reactive astrocytes-specific markers including lipocalin-2 (LCN2) and Serpin Family A Member 3 (Serpina3n), which do not identify non-reactive astrocytes, have been investigated.[19]

Astrocytes play an important role in water and ion homeostasis with AQP4, a family of water channel protein that is distributed along the cell membranes. AQP4 water channels are predominantly localized at astrocytic end-feet processes that contact blood vessels, mediating the water movements between astrocytes and the vascular region (Figure 1.2).[20,21] Localization of AQP4 in astrocytic end-feet processes relies on AQP4 anchoring to the dystrophin associated protein complex (DAPC) consisting of α- and β-syntrophin, α-dystrobrevin, and dystroglycans. Previous findings using animal models that AQP4 is involved in brain pathophysiology including glial scar formation[22] and neuroinflammation[23] have drawn increasing interest in AQP4 distribution and function.

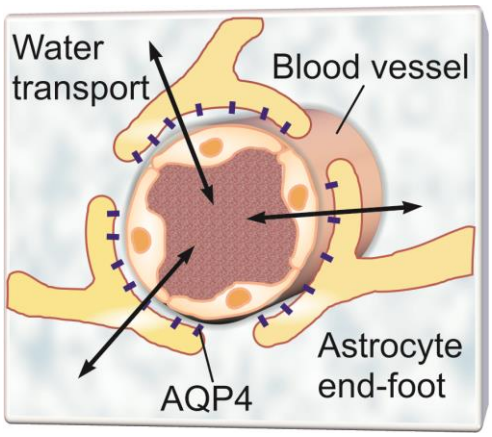

Figure 1.2 Water transport through aquaporin-4 at the blood-brain barrier. Aquaporin-4 (AQP4), water channel protein that controls water transport, is predominantly localized at the end-feet of astrocytes that cover the blood vessel.

1.1.4 In vitro models of the human BBB

The lack of experimental models that can precisely evaluate the interactions between the BBB and CNS drug delivery systems restricts successful clinical translation of therapeutic molecules.[24,25] The complex physiology of animal models makes it difficult to perform mechanistic studies and direct quantitative analysis of the barrier function at molecular and cellular levels in real time.[24] Moreover, cross-species inaccuracy has led to failure of more than 80% of drugs in the translation from animal models to human clinical trials.[26,27] These challenges highlight the importance of developing an *in vitro* model that mimics the essential physiological structure and function of the human BBB and that reproduces the key relationships of healthy and disrupted barrier functions in a controlled manner.

Traditional *in vitro* models use a Transwell culture system that allows for co-culture of multiple cells in separated space and measurement of the endothelial barrier integrity with transendothelial electrical resistance (TEER) or permeability assays. However, these models cannot accurately mimic the physiological microenvironment with their limited ability to incorporate three-dimensional (3D) microenvironment and dynamic shear flow.

In recent years, microengineered physiological systems, combining the fortes of microfluidic technology and tissue engineering, have emerged as an alternative to traditional *in vitro* models with enhanced control over physiologically relevant parameters that are critical in constructing a model for the organ of interest. By allowing researchers to expose human cell lines to physiologically relevant chemical and mechanical cues,[28,29] these biomimetic models provide the means to better balance model simplicity and

physiological complexity when used as preclinical drug screening tools. However, there is currently no physiologically relevant *in vitro* human BBB model that incorporate all the three cell components (endothelial cells, astrocytes, and pericytes) originated from human, 3D astrocytic network, and shear flow. Especially, to date, most *in vitro* BBB models have relied on two-dimensional (2D) culture system and focused on recapitulating the endothelial compartment for studying molecular transport across the brain endothelium.[30-32] Although these 2D models have proved to be useful tools for drug screening, they are marked by the lack of physiological relevance to the 3D microenvironment *in vivo.*[33] For example, when cultured on 2D substrates, astrocytes respond to this abnormal environment and exhibit artificial *in vitro* glial reactivity with increased expression of reactive markers that are upregulated in pathological condition *in vivo.*[34] Moreover, some models do not incorporate shear flow that mimics blood flow inside the brain capillaries, although previous studies have shown that shear stress affects the function of the brain endothelial cells with their increased expression of junctional proteins and higher barrier integrity.[35-37]

Previous *in vitro* BBB-on-chip models are listed in (Table 1.1). (Booth and Kim, 2012)[38] and (Cho et al., 2015)[39] showed *in vitro* BBB models with non-human species such as rat or mouse, limiting the models in addressing species difference between humans and other animals. (Herland et al., 2016)[40] failed to demonstrate a physiologically relevant tri-culture model. (Bang et al., 2017)[41] and (Campisi et al., 2018)[42] showed a 3D tri-culture of brain endothelial cells, pericytes, and astrocytes; however, it remains difficult to validate the barrier function using TEER and assess the vascular and perivascular spaces separately to quantify the molecular distributions. (Park et al., 2019)[43] and (Vatine et al., 2019)[44] showed double-layered culture systems like transwell models with technical advantages to

allow real-time measurement of TEER and direct access to vascular and perivascular space for quantitative assessment of barrier function; however, these models remained restricted to 2D astrocyte culture.

1.1.5 Nanomedicines for CNS therapeutics

Recent advances in nanotechnology have enabled the engineering of nanoparticle (NP)-based platforms for enhanced delivery of therapeutics to the CNS (Figure 1.3).[45-47] NPs are promising CNS delivery systems with multi-functionalization of their surface to interact with the transporters or receptors at the BBB for crossing the BBB. Moreover, their drug loading capacity allows stable circulation for the sustained drug delivery to target sites.

Table 1.1 Previous *in vitro* human blood-brain barrier models.

Refs	Triculture (E+A+P)	Human cell source	3D culture of astrocytes	Shear flow
Booth and Kim, Lab Chip, 2012	x	x	x	o
Cho et al., Sci.Rep., 2015	x	x	o	x
Hawkins et al., Brain.Res., 2015	x	x	o	x
Herland et al., Plos One, 2016	x	o	o	x
Bang et al., Sci.Rep., 2017	x	x	o	x
Campisi et al., Biomat., 2018	o	o	o	x
Vatine et al., Cell stem cell, 2019	o	o	x	o
Park et al., Nat.Comm., 2019	o	o	x	o

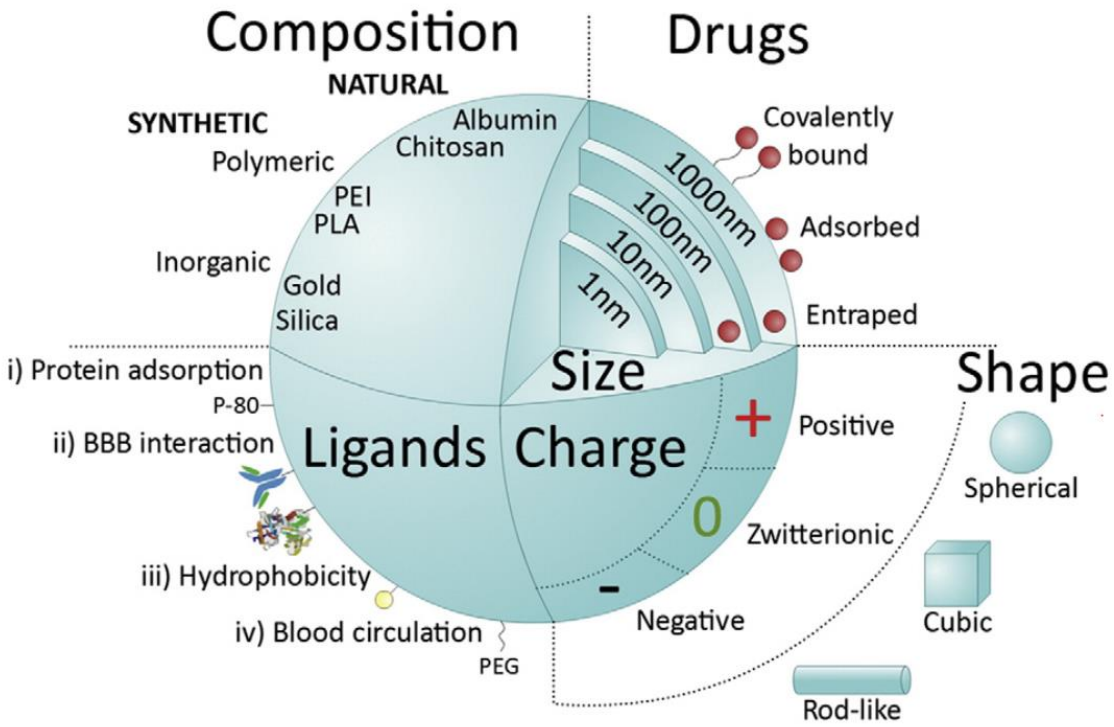

Figure 1.3 Key features of nanoparticles (NPs) for systemic delivery and translocation of the blood brain barrier (BBB).[48] Copyright 2016, Elsevier.

In this regard, various NPs have been developed to deliver therapeutic molecules across the BBB more efficiently.[47] For example, polymeric NPs that have a core polymer matrix, in which drugs can be incorporated, deliver the drugs to the targeted region with high controllability.[49-52] Lipid-based NPs are made with biocompatible and biodegradable lipids that are present in biological membranes, which result in low toxicity in the body.[53-55] Especially, high-density lipoprotein (HDL)-mimetic NPs reconstitute the natural HDLs that are composed of apolipoproteins and phospholipids. In addition, these HDL-mimetic NPs can cross the BBB without additional surface modifications as the apolipoproteins interact with several receptors at the BBB.[56-59]

1.1.5.1 High-density lipoprotein-mimetic nanoparticles for CNS drug delivery

HDL is a natural nanoparticle that transports cholesterols from peripheral tissues to the liver, contributing to the maintenance of lipid metabolism and cholesterol homeostasis in the body.[60] Moreover, HDL transports endogenous microRNAs, vitamins, hormones, and proteins through blood and interstitial fluids to various organs. To facilitate the delivery, HDLs have high stability with long circulation time. In addition, HDLs interact with several receptors expressed on the cell membranes, such as scavenger receptor type B1 (SR-B1), low-density lipoprotein receptor (LDLR) and LDLR-related protein 1 (LRP1). These receptors are highly expressed on brain endothelial cells, and thus, the HDL-mimetic NPs could facilitate the delivery of therapeutic molecules across the BBB via receptor-mediated transcytosis.[56,61,62]

1.2 **Research Objectives**

The low success rate of the CNS drug development is attributed primarily to a unique CNS barrier structure, the blood-brain barrier (BBB). Moreover, a large number of CNS therapeutics fail in clinical trials primarily due to the absence of reliable preclinical models of human BBB. Thus, there is a growing unmet need for a human BBB model that can be used to study the interactions between CNS therapeutics and the BBB. Especially, a model that enables quantitative analysis of drug transport mechanisms and drug distribution at tissue and cellular levels is yet to be developed.

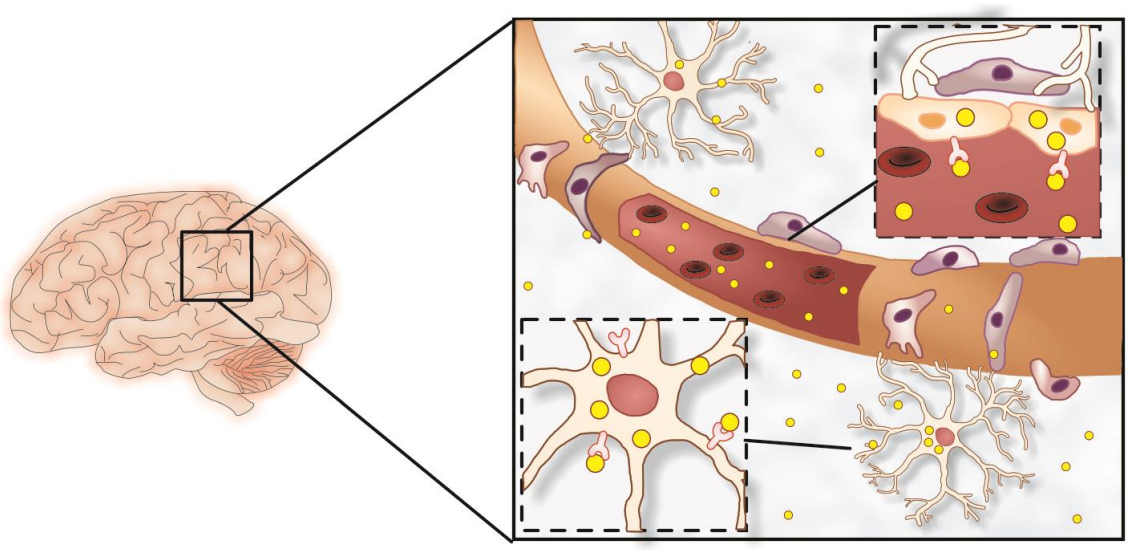

Figure 1.4 Distribution of therapeutic molecules in the brain. Drugs circulating in the blood can cross the BBB via specific receptors or transporters. As a result, the final drug locations in the brain near the BBB can be predicted as follows: (1) in the blood, (2) in cells (brain endothelial cells, pericytes, or astrocytes) (3) in the brain parenchyma (not in cells)

The primary goal of this work is to develop a novel microengineered human BBB model for testing CNS drugs. The new microengineered human BBB platform is designed to incorporate a tight endothelial barrier, shear flow, pericytes that cover the endothelium, and physiological states of human astrocytes in 3D microenvironment. The BBB model is then used for quantitative analysis of nanoparticle transport across the BBB at tissue and cell levels. Ultimately, the model will provide a reliable tool with which drug efficacy can be effectively predicted for complex human CNS diseases while presenting a complementary *in vitro* model to existing *in vivo* models for prescreening drug candidates in a mechanistic manner.

1.3 Thesis Outline

To achieve the primary objectives, the study is divided into the following aims:

Aim 1: Develop a microengineered human BBB model

- Design a microfluidic device to construct the human BBB
- Characterize the specialization of human brain microvascular endothelial cells as constituent cells for the BBB
- Characterize the physiology of astrocytes in 2D and 3D

Aim 2: Characterize the structure and function of the BBB model

- Demonstrate the physiologically relevant structure of the BBB
- Validate the barrier integrity of the model
- Analyze the polarized distribution of aquaporin-4 at the BBB

Aim 3: Evaluate nanoparticle transport and distribution on the BBB model

- Characterize the HDL-mimetic nanoparticles synthesized with microfluidic technology
- Demonstrate the brain penetrance of the HDL-mimetic nanoparticle using a mouse model
- Analyze the transport and distribution of the HDL-mimetic nanoparticles on a chip

CHAPTER 2. DEVELOPMENT OF A MICROENGINEERED HUMAN BLOOD-BRAIN BARRIER MODEL

2.1 Introduction

The blood-brain barrier (BBB) is a highly functionalized vascular border of the central nervous system (CNS) that regulates the transport of substances between the blood and brain.[3] The barrier function is attributed mainly to the unique perivascular structure specialized by a three-dimensional (3D) network of astrocytes that communicate with endothelial cells and pericytes (Figure 1.1).[6] Astrocytes form the glia limitans of the BBB with their end-feet contacting the blood vessels and control the influx of water through aquaporin-4 (AQP4).[13,14] Pericytes embedded in the basement membrane wrap around the endothelium and contribute to astrocytic polarization.[10] These complex cellular interactions at the BBB maintain its integrity and restrict the penetration of drugs, leading to a low success rate in the development of therapeutics for CNS diseases.[5]

It is important to understand the functionality of the perivascular structures and their interactions with the brain microvessels to study the selective barrier function of the BBB which may ultimately lead to develop more effective CNS drugs that can permeate into the brain. However, the lack of experimental models that can precisely evaluate the interactions between the BBB and delivery carriers restricts successful clinical translation of CNS drugs.[24,25] Animal models often do not predict drug responses in humans due to species differences.[26,63,64] Moreover, the complex physiology of animal models makes it difficult to perform mechanistic studies and direct quantitative analysis of CNS drugs with

the barrier at molecular and cellular levels in real time.[24] These challenges highlight the importance of developing an *in vitro* model that mimics the essential physiological structure and function of the human BBB and that reproduces the key relationships of healthy and disrupted barrier functions in a controlled manner.

Recent advances in organ-on-a-chip technology have provided the ability to recapitulate the microenvironment of the BBB.[65,66] Existing *in vitro* human BBB-on-chip models have made efforts to reconstitute the tight endothelial barrier function using several platforms that include monoculture of brain endothelial cells[39] and co-culture of endothelial cells with astrocytes in two-dimensional (2D)[38] and 3D[40,41] microenvironments. A recent BBB model with 3D culture of endothelial cells, pericytes, and astrocytes[42] enabled reconstitution of direct cellular interactions, resulting in the barrier function with permeability lower than previous *in vitro* models of monoculture or co-culture. However, it remains difficult to incorporate the complex physiology of astrocytes into the *in vitro* BBB models and demonstrate the contribution of astrocytes to the BBB's health and disruption. In a healthy brain, astrocytes show branched processes around their cell bodies.[67] In response to CNS injuries or diseases, astrocytes become reactive, which contributes to BBB breakdown and disease progression such as neurodegeneration, ischemia, and infection.[17,18] Reactive astrocytes undergo changes in morphology and gene expressions including lipocalin-2 (LCN2) and Serpin Family A Member 3 (Serpina3n).[19] *In vitro* BBB models thus would be enhanced and widely useful for CNS disease modeling if healthy and reactive astrocytes could be reconstituted in a controlled manner.

Here, we design a microengineered physiological system to model the human BBB with specialized brain endothelial cells and 3D astrocytic network (Figure 2.1). The BBB-

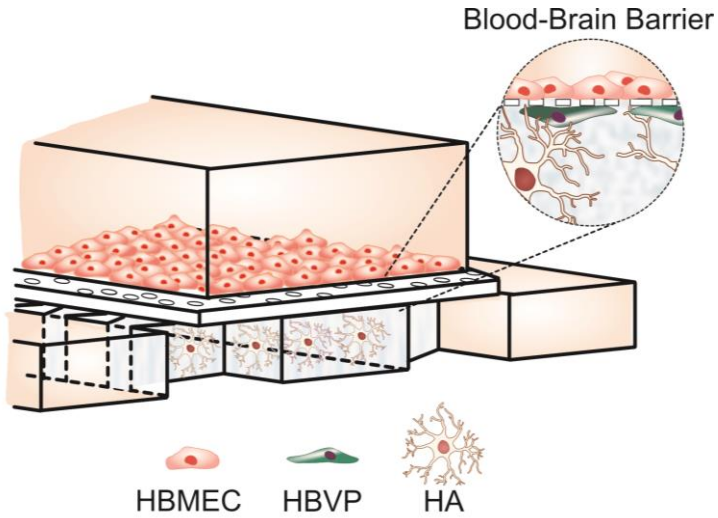

Figure 2.1 Schematic of the microengineered human blood-brain barrier chip

specific characteristics of the human brain microvascular endothelial cells (HBMECs) are analyzed with their gene expression of BBB-specific markers. To demonstrate physiological characteristics of astrocytes in 3D, we analyze their expressions reactive astrocyte markers as well as morphologies. In particular, decrease in expression of LCN2, a strong reactive astrocyte-specific marker which is expressed only in reactive astrocytes in many diseases such as neuroinflammation and stroke, provide evidence of reduced reactive gliosis of astrocytes.[19] We then set up the co-culture protocol for reconstitution of the BBB in our microfluidic device. Our microfluidic chip will provide a culture platform to reconstitute the human BBB consisting of specialized brain endothelium and 3D network of astrocytes with reduced reactive gliosis.

2.2 Results and Discussions

2.2.1 Design a platform for a microengineered human BBB

Our microengineered human BBB model is designed to reconstitute the BBB structure with the brain vascular endothelium and human brain vascular pericytes

(HBVPs) in direct contact with 3D network of human astrocytes (HAs) (Figure 2.1). The BBB chip has two compartmentalized microfluidic channel layers that combine a 2D endothelial monolayer with a 3D brain microenvironment, enabling highly sensitive quantification of molecular distribution in each space independently (Figure 2.2a,b). The upper layer of the device mimics the vascular space of the brain microvasculature where an endothelial monolayer is formed on a 7 μm thick porous membrane (8 μm diameter pores at a density of 1E5 pores/cm^2) with 16 μL/min of continuous fluid flow (shear stress: 4 dyne/cm^2). The lower layer accommodates pericytes underneath the membrane and astrocytes in a 3D Matrigel (5 mg/mL) in the center channel along with the two side channels (Figure 2.2c). This structure allows for the 3D astrocyte culture in a hydrogel that is inserted into the center channel and is stably maintained by surface tension. Importantly, the edges of the upper channel are aligned to cover the both-side arrays of micropillars (Figure 2.2d) to avoid the undesirable leakage that may occur in the edge of a endothelial monolayer at the channel walls, which we recently demonstrated with a microfluidic transcellular monitor.[68] The device is designed to have sufficient diffusive transport of culture medium components into the hydrogel channel within 1 hour of media refreshment in the upper and the two side channels (Figure 2.2e and Figure S 2.1). Moreover, the two side channels promote independent lateral perfusion through the hydrogel enabling efficient removal of metabolic wastes or unbound antibodies and, more importantly, provide the opportunity to precisely sample solutions perfused from the hydrogel without disturbing the cellular organization.

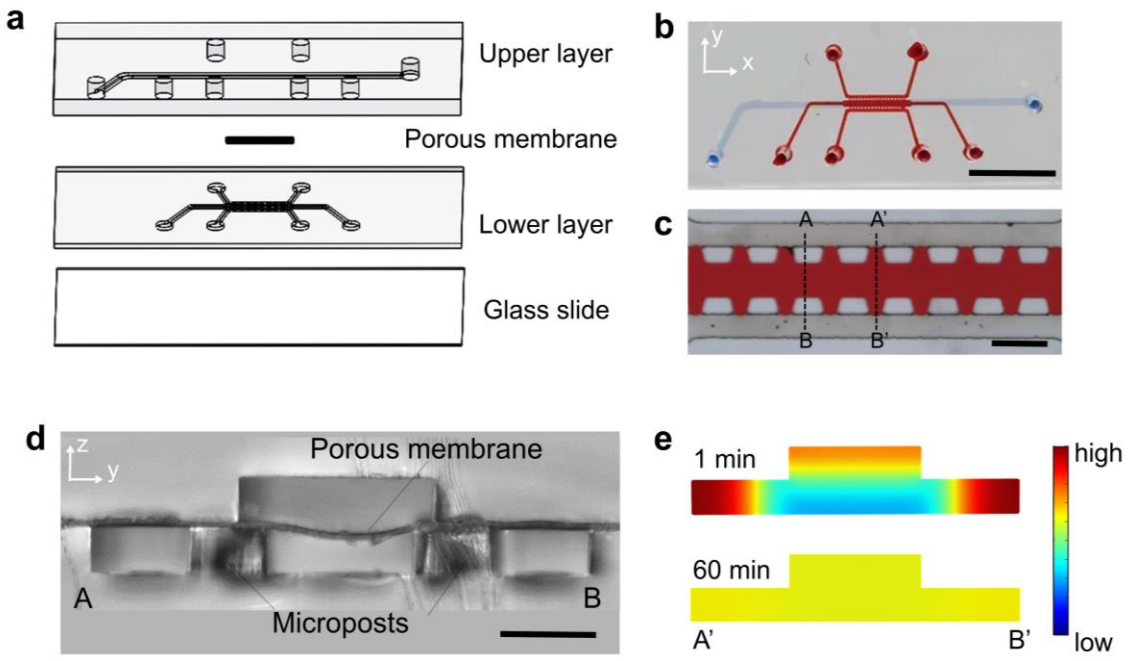

Figure 2.2 Structure of the microengineered chip. a, Explosion view of the device consisting of upper vascular layer, porous membrane, lower perivascular layer, and glass slide. **b**, A photo of the device after completing fabrication of the device (blue: upper channel and red: lower channels) (scale bar = 500 μm). **c**, Lower layer consisting of three parallel channels separated by series of micropillars (red: center channel) (scale bar = 500 μm). **d,** Cross section of the device after fabrication (along A-B in Fig. 1c) (scale bar = 200 μm). **e,** Serum transport into the 3D Matrigel in the device after 1 min and 60 min of media infusion into the upper and two side channels (along A'-B' in Fig. 1c).

2.2.2 Selection of co-culture medium

Since three different types of cells (HBMEC, HBVP, and HA) are co-cultured in a device which share the culture environment, the co-culture medium should be selected to provide the optimal culture microenvironment to all three types of cells. Morphologies and metabolic activities of cells cultured in each cell culture medium (E, endothelial cell medium; A, astrocyte medium; P, pericyte medium; M, microglia medium; G, glia medium (A+M)) and mixture of the culture medium were assessed over 3 days of culture to screen

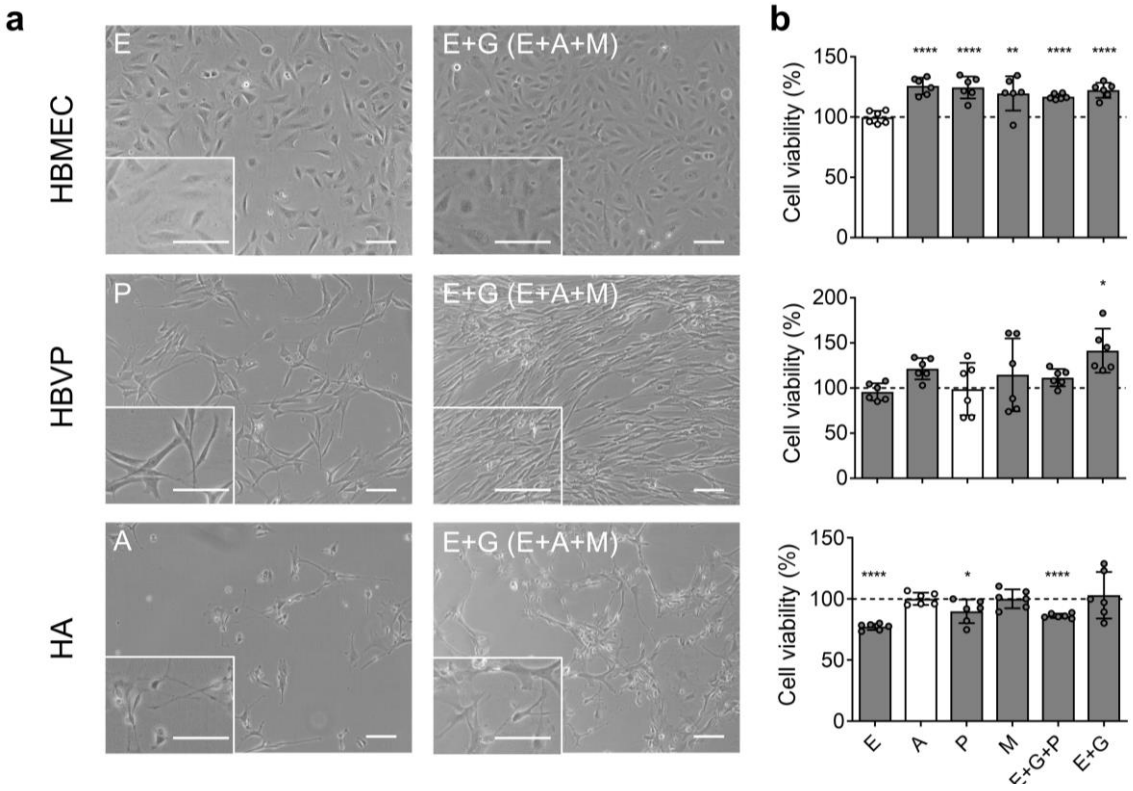

Figure 2.3 Selection of co-culture medium for BBB tri-culture model. a, Morphologies of HBMEC, HBVP, and HA in their respective culture medium and mixed medium (E+G). **b,** Metabolic activities of HBMEC, HBVP, and HA cultured in Endothelial cell medium (E), Astrocyte medium (A), Pericyte medium (P), Microglia medium (M), E+ G (E:A:M= 1:1:1:1), and E+P+G (E:P:A:M=1:1:1:1) (*p<0.05, **p<0.01, and ****p<0.001).

the cell conditions. Here, microglia medium was included to develop a better neurovascular unit system including the current BBB model, in which microglia will be co-cultured for future studies. Morphology of cells were not significantly different between the cells cultured in each culture medium and in the mixed culture medium (E+G) (Figure 2.3a). Moreover, all three types of cells showed high cell metabolic activities in the mixed culture medium (E+G) after 3 days of culture, which were quantified by a (3-(4,5-dimethylthiazol-2-yl)-5-(3-carboxymethoxyphenyl)-2-(4-sulfophenyl)-2H-tetrazolium) (MTS) assay (Figure 2.3b).

2.2.3 Verification of endothelial specialization for the BBB function

The brain vascular endothelium is a highly specialized gatekeeper with complex transport mechanisms.[5,9] The critical barrier function of the BBB endothelium is reportedly characterized by high expressions of BBB-specific proteins[69,70], including junctional, transporter, and receptor proteins and by high transendothelial electrical resistance (TEER) (i.e., low permeability).[71] In addition, applications of specific human cell sources have enhanced the physiological relevance of *in vitro* models to the unique properties of the BBB endothelium.[42] In our present study, thus, we first demonstrated that our brain-specific endothelial cells, when cultured with the other BBB cells (i.e., astrocytes and pericytes), exhibited increases in representative gene expressions including proteins that regulate junctional formation, carrier-mediated transport, active efflux, and amyloid beta (Aβ) transport (Figure 2.4a). Especially, BBB cellular interactions upregulated the endothelial gene expressions of the representative junctional proteins such as occludin (OCLN), zonula occludens-1 (ZO-1), and vascular endothelial cadherin (VE-cad) (Figure 2.4b) and the representative membrane transporters and receptors including glucose transporter 1 (GLUT1), cholesterol efflux regulatory protein (CERP; ATP-binding cassette sub-family A member 1, ABCA1), and low-density lipoproetin receptor-related protein 1 (LRP1) (Figure 2.4c).

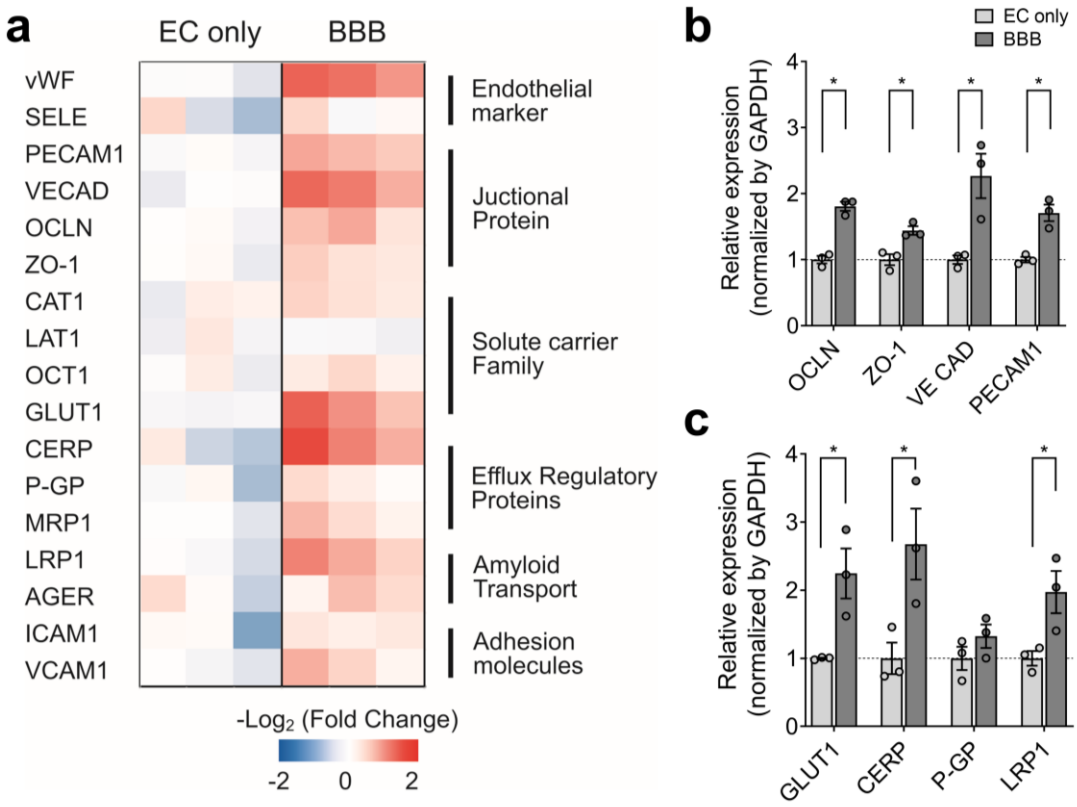

Figure 2.4 Gene expressions of the immortalized human brain microvascular endothelial cells in monoculture and triculture models. a, Heat map of RT-qPCR results of HBMECs in monoculture and tri-culture systems (n=3 for each condition). **b,c,** Gene expression of HBMECs in monoculture and tri-culture systems including junctional proteins (**b**) and receptor proteins (**c**) (n=3 for each condition, *p<0.05).

2.2.4 Effects of shear stress on endothelial function

Brain endothelial cells in brain capillary are exposed to a continuous fluidic shear stress in a range of 4 ~ 20 dyne/cm^2.[72] Blood flow in the blood vessel results in shear stress on the vessel wall in the direction of flow. Previous studies have demonstrated that shear stress plays an important role in regulating brain endothelial function, including junctional protein expressions[35-37] and barrier integrity[35,37]. We verified the effects of shear stress on the brain endothelium constructed with HBMECs in a microfluidic channel. In our microfluidic device, a physiological level of shear stress was responsible for inducing endothelial function with efflux transporter protein expression (Figure 2.5a), and endothelial nitric oxide synthase (eNOS) phosphorylation (Figure 2.5b,c).

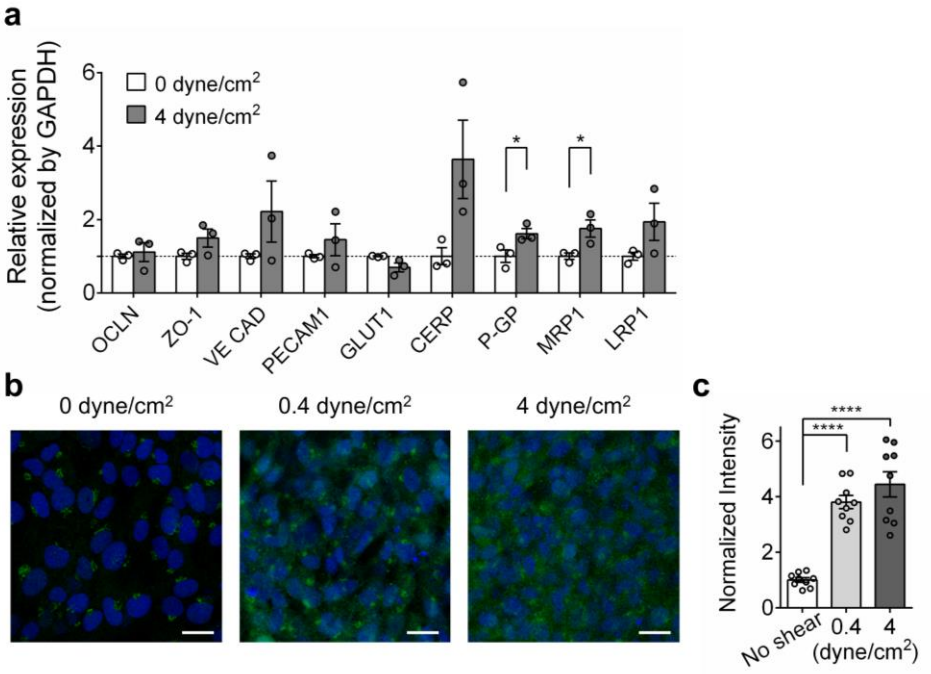

Figure 2.5 Shear effect on the brain endothelium. a, Gene expressions of HBMECs in monoculture under static condition (Transwell) and physiological level of shear stress (chip, 4 dyne/cm^2). **b,** Confocal images of HBMECs from different shear stress conditions labelled with phospho-eNOS (Ser1177) (eNOS, green; DAPI, blue) (scale bars = 20 μm). **c,** Fluorescence intensities of eNOS from confocal images normalized by the average intensity of the static condition (n=9 for each condition, ****p<0.001).

2.2.5 In vivo-like morphology of 3D-cultured astrocytes

Not only is the vascular endothelial barrier function important to developing and validating *in vitro* BBB models, the physiological relevance provided by perivascular regions is also essential to precisely recapitulate the BBB structure and function. One difficult yet important element in reconstituting the BBB is to preserve the morphological and physiological characteristics of healthy astrocytes.[16] Astrocytes reportedly restore their *in vivo*-like physiological properties such as morphology and functional reactivity in 3D culture systems.[34,67] We confirmed that HAs cultured on a 2D Matrigel-coated surface were flat and polygonal in shape (Figure 2.6a,c). However, HAs cultured in 3D Matrigel exhibited more *in vivo*-like ramified morphology (Figure 2.6b,d). Moreover, the majority of HAs cultured in 3D featured small cell bodies with radially distributed thin and long branches, whereas HAs cultured in 2D exhibited enlarged cell bodies with less and short processes (Figure 2.6e,f).

2.2.6 Reduced reactive gliosis of 3D-cultured astrocytes

Reactive astrocytes are characterized by changes in gene expression as well as morphology. We performed quantitative analysis on the gene expression of reactive gliosis markers that are upregulated in pathological conditions to support that 3D cultured HAs in our BBB chip are more physiologically relevant than conventional 2D culture systems. In particular, LCN2 plays an important role in neuroinflammation by mediating proinflammatory responses in injury.[73] We found that reactive gliosis markers, vimentin (VIM) and LCN2, were downregulated in HAs cultured in 3D compared to those cultured in 2D, while the level of glial fibrillary acidic protein

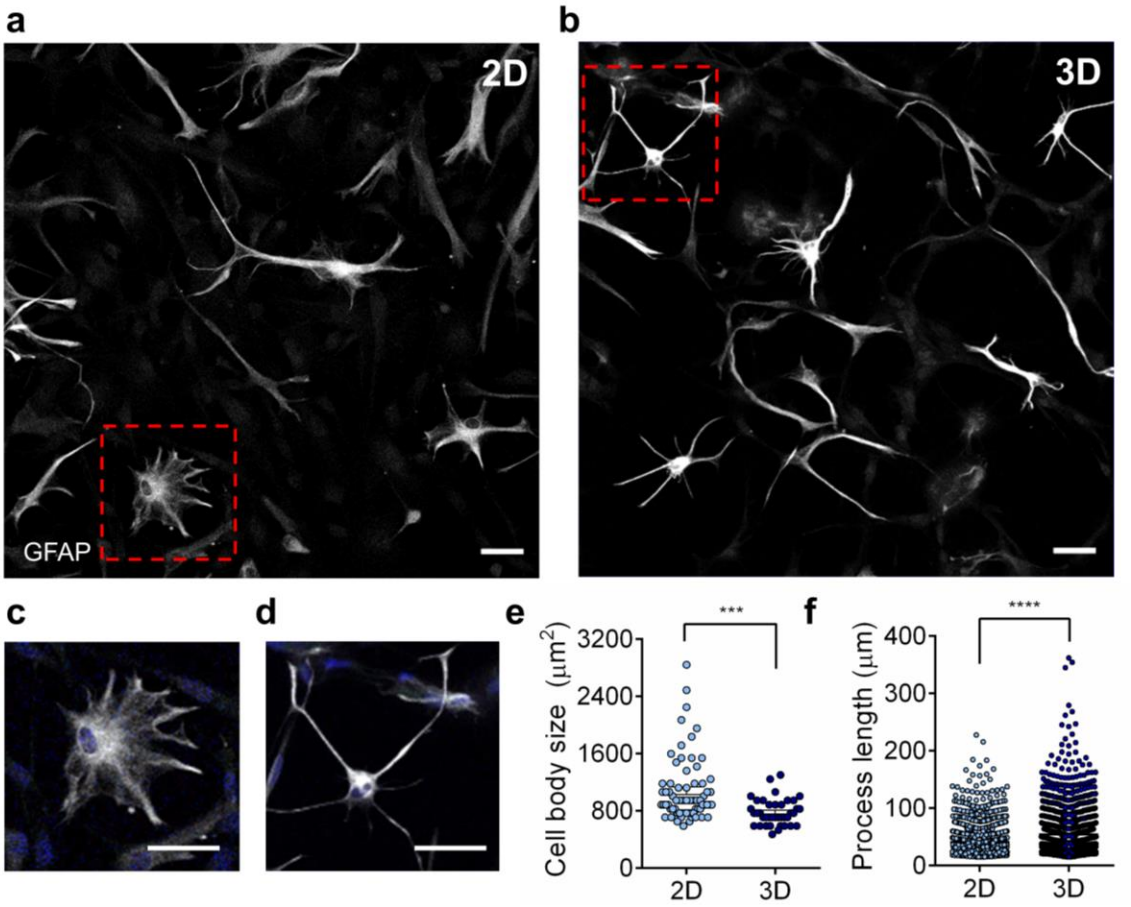

Figure 2.6 Morphologies of human astrocytes (HA) cultured on 2D Matrigel coated surface and in 3D Matrigel. a, HAs cultured on 2D Matrigel coated surface showed flat polygonal shapes. **b,** HAs cultured in 3D Matrigel exhibited small cell bodies with radial distribution of long cellular processes. **c,d,** Representative morphology of human astrocyte (HA) cultured on Matrigel-coated 2D surface (**c**) and in 3D Matrigel (**d**) (scale bars = 50 μm). **e,** Cell body size of HAs cultured in 2D and 3D (n=69 for 2D and 39 for 3D, ***p<0.005). **f,** Process length of HAs cultured in 2D and 3D (n=1352 for 2D and 1302 for 3D, ****p<0.001). Scale bars = 50 μm.

(GFAP), the representative astrocyte marker, did not significantly change (Figure 2.7a). In addition, we confirmed that the LCN2 expression level could be further regulated in a dose-dependent manner in response to an inflammatory cytokine treatment with interleukin-1β (IL-1β) in the 3D culture as in 2D (Figure 2.7b,c). These results demonstrate the physiological relevance of 3D cultured HAs and indicate the potential

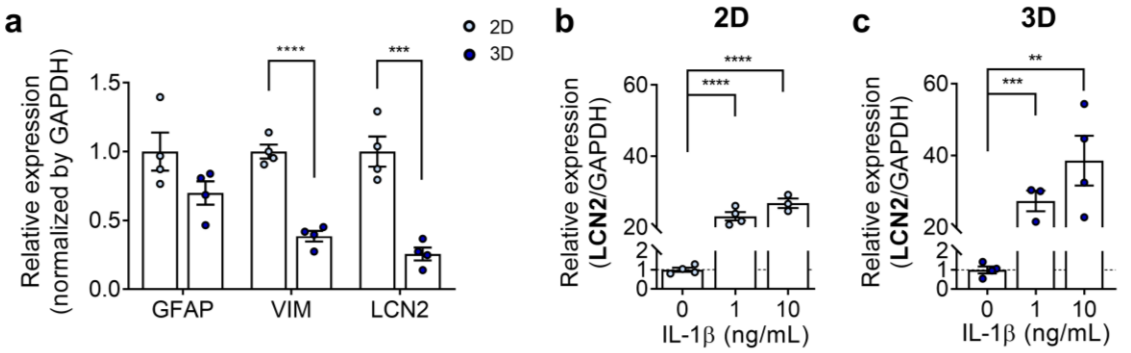

Figure 2.7 Reactive gliosis marker expressions of astrocytes cultured in 2D and 3D. a, Gene expression of reactive gliosis markers in HAs cultured in 2D and 3D (n=4 for each condition, ***p<0.005 and ****p<0.001 by student t test). **b,c,** Gene expression of LCN2 in HAs cultured on Matrigel-coated 2D surface (**b**) and within 3D Matrigel (**c**) with IL-1β treatment demonstrating the ability to model reactive astrocytes more effectively in 3D (n=4 for each condition, **p<0.01, ***p<0.005, and ****p<0.001).

application of our BBB chip for reactive astrogliosis modeling such as in neuroinflammation.

2.3 **Conclusions**

Recent *in vitro* models have demonstrated the importance of cell source to mimic organ-specific fuction *in vitro*, as well as for human disease modeling.[74,75] In particular, highly complex BBB organization requires brain-specific cells to be sourced appropriately for *in vitro* modeling, which secures the key characteristics including the tight barrier function and low permeability resulting from high expressions of BBB-specific proteins[5,9,69,70], compared to human umbilical vein endothelial cells (HUVECs) widely used in previous models[41,76] that may not closely recapitulate the unique properties of the brain endothelium.[77] Immortalized human brain endothelial cells are good candidates for standardized screenings due to their availability as well as

indefinite proliferation while preserving their properties. Previous studies using hCMEC/D3 in microfluidic BBB models showed their barrier function with junctional protein expression, TEER[31], and permeability[76]. In our present study, we have used HBMEC as it has been reported that HBMEC is the most suitable and promising immortalized human brain endothelial cell line among the four available cell lines (hCMEC/D3, HBMEC, TY10, and BB19) for *in vitro* modeling of human BBB in terms of the barrier tightness and permeability.[78] Moreover, the use of HBMECs validated their BBB-specific function with their increased gene expressions of BBB-specific proteins in the presence of pericytes and astrocytes.

Our BBB chip is designed to incorporate 3D culture of HAs into the cellular organization in order to recapitulate the BBB physiology and integrity. We first demonstrated reduced astrogliosis in 3D cultured HA with the decreased expression of reactive gliosis markers as well as the *in vivo*-like morphology. A recent significant study has shown that LCN2 is a reactive astrocyte-specific marker that is commonly induced in pathological conditions, whereas intermediate filament proteins such as GFAP and VIM are normally expressed by astrocytes in both physiological and pathological conditions.[19] We demonstrated that LCN2 expression in HAs cultured in 3D was lower than in those cultured on 2D and more importantly that IL-1β treatment was more effective in 3D than in 2D, indicating the greater value for neuroinflammation modeling. Our results suggest that the cells restore their normal responses in 3D, while they are already reactive in 2D culture without external stimulation, revealing that studies that have used astrocyte in 2D culture may have overlooked the potential reactivity in their model. Taken together, our model will establish the physiologically

relevant human BBB with the ability to control status of astrocytes from resting to reactive conditions as a potential for modeling of neuroinflammation and reactive gliosis in CNS diseases.

2.4 Materials and Methods

Fabrication of the microfluidic device. The microfluidic device was fabricated with polydimethylsiloxane (PDMS; Sylgard 184; Dow Corning, Midland, MI, USA) using soft lithography.[79] To create the PDMS slab for the upper layer, PDMS pre-polymer (10:1 elastomer base to curing agent, wt/wt) was degassed and poured onto silicon wafers patterned with SU-8 (Microchem, Newton, MA, USA). The thin PDMS sheet for the lower layer of the device was created by spin coating an SU-8 patterned silicon wafer with a PDMS pre-polymer to a height of 250 μm. After curing the PDMS pre-polymer for 1 h at 80˚C, inlets and outlets of the channels were formed with 1 mm diameter biopsy punch. A polycarbonate membrane (8 μm pore; Sterlitech Corp, Kent, WA, USA) treated with 5% 3-aminopropyl-trienthoxysilane (APTES) solution (Sigma-Aldrich, St. Louis, MO, USA)[80] was sandwiched and bonded between the upper and lower PDMS layers using a plasma cleaner (Harrick Plasma, Ithaca, NY, USA). The fabricated device was then placed in a polystyrene box (Ted Pella Inc., Redding, CA, USA). The device and microchannels are sterilized with 70% ethanol and placed in a dry oven at 80˚C for 2.5 days to restore hydrophobicity of the PDMS surface.

Computational fluid dynamics. Serum transport in the microfluidic channels was modeled with COMSOL (COMSOL, Multiphysics 5.3a, Stockholm, Sweden). The convection-diffusion equation was solved using the chemical species transport module.

The diffusion coefficient of serum was assumed to be 5.9×10^{-11} m^2/s in culture medium[81], and 8.0×10^{-11} m^2/s in Matrigel[82]. The initial serum concentrations of culture medium and Matrigel was taken as 5×10^{-3} mol/m^3 and 0 mol/m^3, respectively. Matrigel and the porous membrane were defined as a porous medium with porosity value of 0.8 and 0.016, respectively. The computational simulation was performed within a microfluidic device without cellular components. The three-dimensional model was used with no-slip boundary conditions on all the walls, and the numerical grid for performing the simulations consisted of approximately 850,000 finite elements.

Cell culture. Immortalized human brain microvascular endothelial cells (HBMEC; Innoprot, Bizkaia, Spain) at passage 5-10 were maintained in endothelial cell medium (Sciencell, San Diego, CA, USA) on flasks coated with 50 μg/mL fibronectin (Sigma Aldrich). Human brain vascular pericytes (HBVP) and human astrocytes (HA) (Sciencell) were cultured on 1 mg/mL poly-l-lysine (PLL, Sigma Aldrich) coated flasks and maintained in astrocyte and pericyte medium, respectively (Sciencell). Both primary cells between passages 3 and 5 were used for all experiments. Fibronectin and PLL coating procedures were achieved following the manufacturer's instruction. To optimize cell culture condition, cell metabolic activity in different medium condition were quantified using a (3-(4,5-dimethylthiazol-2-yl)-5-(3-carboxymethoxyphenyl)-2-(4-sulfophenyl)-2H-tetrazolium) (MTS) assay (n = 6), which measures the formazan product by cell metabolic activity. CellTiter 96 AQueous One Solution Cell Proliferation Assay (Promega, Madison, WI, USA) was added to HBMECs, HBVPs, and HAs cultured in Endothelial cell medium (E), Astrocyte medium (A), Pericyte medium (P), Microglia medium (M; Sciencell), E+ G (E:A:M= 1:1:1:1), and E+P+G (E:P:A:M=1:1:1:1) after 3 days of culture.

Here, we describe 1:1 mixture of A and E as glial cell medium (G). After 4 h of incubation, the optical absorbance of each sample was measured at 490 nm using Cytation 5 plate reader (BioTek, Winooski, VT, USA). To compare HAs in 2D and 3D, HAs were seeded at a density of 1 x 10^6 cells/mL in Matrigel coated 24 wells and in 3D Matrigel (5 mg/mL). After 1 day of culture, cells were stimulated with 1 ng/mL and 10 ng/mL of recombinant human interleukin 1-beta (IL-1β; Gibco, Grand Island, NY, USA) and incubated for another 20 h for analysis.

Transwell culture. Prior to seeding HBVPs on the insert membrane (facing down), the bottom surface of the membrane in the insert was coated with 50 µg/mL fibronectin (Sigma-Aldrich) for 1 h at 37 ˚C while the insert was placed upside down. Then HBVPs were seeded at 1 x 10^7 cells/mL density on the membrane and incubated for 6 h to allow adhesion of cells onto the fibronectin-coated membrane. Then 1 x 10^7 HAs were seeded into the well. Transwell was placed in the incubator at 37 ˚C for 6 h, and the insert was coated with 50 µg/mL fibronectin for 1 h at 37 ˚C. HBMECs were then seeded in the insert with the density of 7 x 10^7 cells/mL. Cells were then co-cultured for 48 h before collecting mRNA.

Real-time quantitative reverse transcription polymerase chain reaction (Real-time qRT-PCR). Cell-specific gene expressions were quantified by qRT-PCR analysis. Briefly, total RNA from HBMECs and HAs were isolated and collected using the RNeasy Mini kit (Qiagen GmBH, Hilden, Germany). The amount of collected RNA samples were measured by Cytation 5 plate reader and 800 ng (HBMEC) and 280 ng (HA) of RNA were reverse-transcribed into cDNA with T100^{TM} Thermal Cycler (Bio-Rad, Hercules, CA, USA) using High-capacity cDNA Reverse Transcription kit (Applied Biosystems, Foster City, CA,

USA). To analyze endothelial specific gene expressions in HBMECs (n = 3), microfluidic qRT-PCR was performed with Flex Six IFC (Fluidigm Corp., South San Francisco, CA, USA) using the Fluidigm Biomark system (Fluidigm). To analyze glial reactivity of HA in 2D and 3D culture system (n = 4), standard qRT-PCR was performed with a StepOnePlus Real-Time PCR system (Applied Biosystems) using TaqMan Fast Universal PCR Master Mix (Applied Biosystems). The target genes were assessed using commercially available primers (All primers listed in Table S 2.1; Applied Biosystems). The results were quantified by the comparative C_t method. C_t values for samples were normalized to the expression of the housekeeping gene, glyceraldehyde 3-phosphate dehydrogenase (GAPDH; Applied Biosystems).

Immunocytochemistry. To visualize cell-specific marker expression, immunocytochemistry was performed. Briefly, samples were fixed with 2% paraformaldehyde (PFA; Santa Cruz Biotechnology, San Diego, CA, USA) for 15 min at RT. After permeabilizing in 0.1% Triton X (Sigma-Aldrich) in PBS for 15 min, the samples were blocked with 2% bovine serum albumin (BSA; Sigma-Aldrich) in PBS for 1 h at RT. Subsequently, the samples were incubated with primary antibody (anti-GFAP (1:200; Invitrogen, Carlsbad, CA, USA)) at 4 ˚C overnight, washed three times with 1% BSA. Then samples were incubated with fluorescence-conjugated secondary antibody (chicken anti-mouse AlexaFluor 594) (1:200; Invitrogen) for 6 h at 4 ˚C to visualize targets. Nuclei were counterstained with 4,6-diamino-2-phenylindole (DAPI; Invitrogen) and stored in PBS before imaging. Fluorescently visualized samples were examined using a confocal microscope (LSM 700, Carl Zeiss, Oberkochen, Germany).

Image analysis. Quantitative analysis of cell morphology was performed using ImageJ (NIH, Bethesda, MD, USA). To analyze the morphology of HAs, the boundaries of cells were obtained automatically using magic wand tool on the maximal intensity projection image.

2.5 **Supplementary Information**

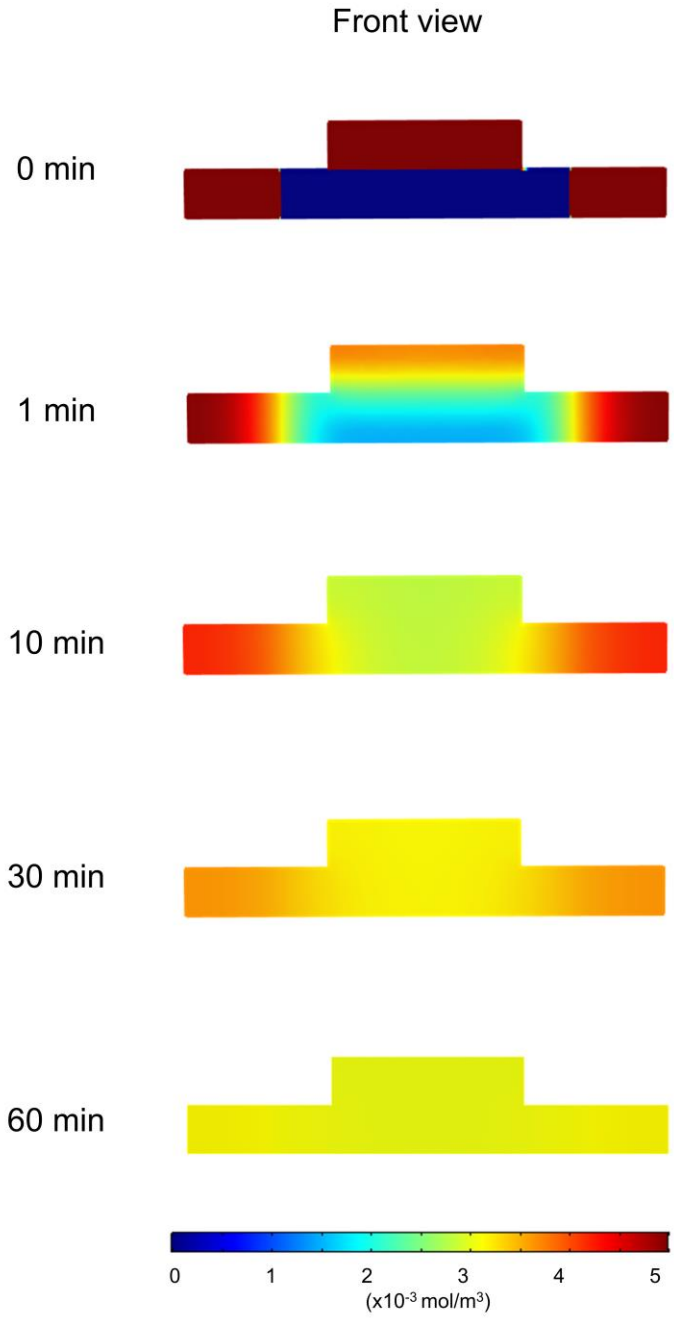

Figure S 2.1 Computational fluid dynamic simulation of nutrient supply into the hydrogel channel over 1 h. Computational predictions of serum transport into the hydrogel channel (lower center channel).

Table S 2.1 Primers/probes information. The target genes were assessed using commercially available primers and probes.

Experiment	Gene Symbol	Gene Name	TaqMan Assay ID #
	GAPDH	Glyceraldehyde-3-phosphate dehydrogenase	Hs02786624_g1
HA RT-qPCR	GFAP	Glial fibrillary acidic protein	Hs00909233_m1
	VIM	Vimentin	Hs00958111_m1
	LCN2	Lipocalin-2	Hs01008571_m1
HBMEC Fluidigm	vWF	von Willebrand factor	Hs01109446_m1
	SELE	E-selectin	Hs00174057_m1
	PECAM1	Platelet and endothelial cell adhesion molecule 1	Hs01065279_m1
	VECAD	Vascular endothelial cadherin	Hs00170986_m1
	OCLN	Occludin	Hs00170162_m1
	ZO-1	Zonula occludens-1	Hs01551861_m1
	CAT1	Cationic amino acid transporter 1 (SLC7A1)	Hs00931450_m1
	LAT1	L-type amino acid transporter 1 (SLC7A5)	Hs00185826_m1
	OCT1	Organic cation transporter 1(SLC22A1)	Hs00427552_m1
	GLUT1	Glucose transporter 1 (SLC2A1)	Hs00892681_m1
	CERP	cholesterol efflux regulatory protein (ABCA1)	Hs01059137_m1
	P-GP	P-glycoprotein 1 (ABCB1)	Hs00184500_m1
	MRP1	Multidrug resistance-associated protein 1 (ABCC1)	Hs01561483_m1
	LRP1	LDL receptor related protein 1	Hs00233856_m1
	AGER	Advanced glycosylation end-product receptor	Hs00179504_m1
	ICAM1	Intercellular adhesion molecule 1	Hs00164932_m1
	VCAM1	Vascular cell adhesion molecule 1	Hs01003372_m1

CHAPTER 3. CHARACTERIZATION OF THE STRUCTURE AND FUNCTION OF THE MICROENGINEERED HUMAN BLOOD-BRAIN BARRIER MODEL

3.1 Introduction

The blood-brain barrier (BBB) is a highly functionalized vascular structure of the central nervous system (CNS) that controls transport of biological substances and immune cells between the central nervous system and the peripheral blood.[6,72] This barrier function of the BBB is attributed to the highly specialized perivascular structure of the BBB, which consists of pericytes, astrocytic end-feet, and a basement membrane.[4] Pericytes that wrap around the endothelium also have been shown to induce polarization of astrocytic end-feet surrounding the brain endothelium.[10] Astrocytes constructing a three-dimensional (3D) perivascular network form the glia limitans of the BBB with their end-feet contacting the blood vessels and control water influx at the BBB through the water channel aquaporin-4 (AQP4).[13,83,84] These complex and dynamic cellular interactions at the BBB maintain the BBB integrity, restricting the penetration of drug and leading to a low success rate in the delivery of therapeutics for CNS diseases.[5]

Therefore, it is critical to develop an *in vitro* BBB model that can include all these required factors for better applications in drug screening and disease modeling. In recent years, microengineered physiological systems, combining the fortes of microfluidic technology and tissue engineering, have emerged as an alternative to traditional *in vitro* models with enhanced control over physiologically relevant parameters that are critical in

constructing a model for the organ of interest. By allowing researchers to expose human cell lines to physiologically relevant chemical and mechanical cues,[28,29] these biomimetic models provide the means to better balance model simplicity and physiological complexity when used as preclinical drug screening tools. Existing *in vitro* human BBB-on-chip models have largely focused on modeling the endothelial barrier system,[38,41,85] which is the representative physiological characteristics of the BBB. However, recent studies have reported that not only the barrier function of the brain endothelium but also the phenotypic characteristics of perivascular cells like astrocytes have to be well recapitulated to develop an in vitro human BBB model.[86,87]

Our BBB model will provide unprecedented capabilities to reproduce key structural and functional characteristics of the human BBB by incorporating the specialized endothelium, pericytes that cover the endothelium, 3D astrocytic network in physiologically relevant extracellular matrix (ECM) material, and shear flow. Importantly, our BBB chip creates a 3D astrocytic network with polarized expression of AQP4. The BBB chip will enable visualization of the 3D cellular network at high spatial resolution and quantitative analysis of permeability.

3.2 Results and Discussions

3.2.1 Microengineered human BBB with 3D astrocytic network

We developed a high-throughput co-culture protocol (Figure S 3.1 and Figure S 3.2), with which we were able to establish the human BBB integrity after 2.5 days of culture,

as the culture time was also suggested and validated in previous studies.[38,85] First, HBVPs were seeded into the center channel of the lower layer, which is coated with fibronectin, while the device is placed upside down. After culturing HBVPs to allow their attachment to the porous membrane, primary HAs, suspended in a Matrigel solution, were seeded into the same channel that HBVPs are cultured. Following gelation in a microfluidic channel, culture medium was filled into the two side channels to avoid the gel drying out. HBMECs were cultured into the upper luminal layer of the device to construct an endothelial monolayer. Twenty-four hours after seeding, culture medium was perfused through the luminal channel at 16 μL/min for another 24 hours to mimic fluid flow and shear stress applied to the brain endothelium.

Our BBB model reproducibly maintains the 3D network of HAs with physiologically relevant morphology underneath the endothelial monolayer and across the lower channel layer (Figure 3.1a,b). The monolayers of HBMECs and HBVPs on the opposite sides of the 7 μm-thick porous membrane (Figure 3.1c) while the proximity and perfusable structure allow for the paracrine and juxtacrine signaling between the three cells. More importantly, our BBB chip clearly demonstrated for the first time in *in vitro* BBB models that HAs in a 3D network extend their end-feet with higher AQP4 and α-syn expressions right underneath the porous membrane over the basal side of the endothelium (Figure 3.1d).

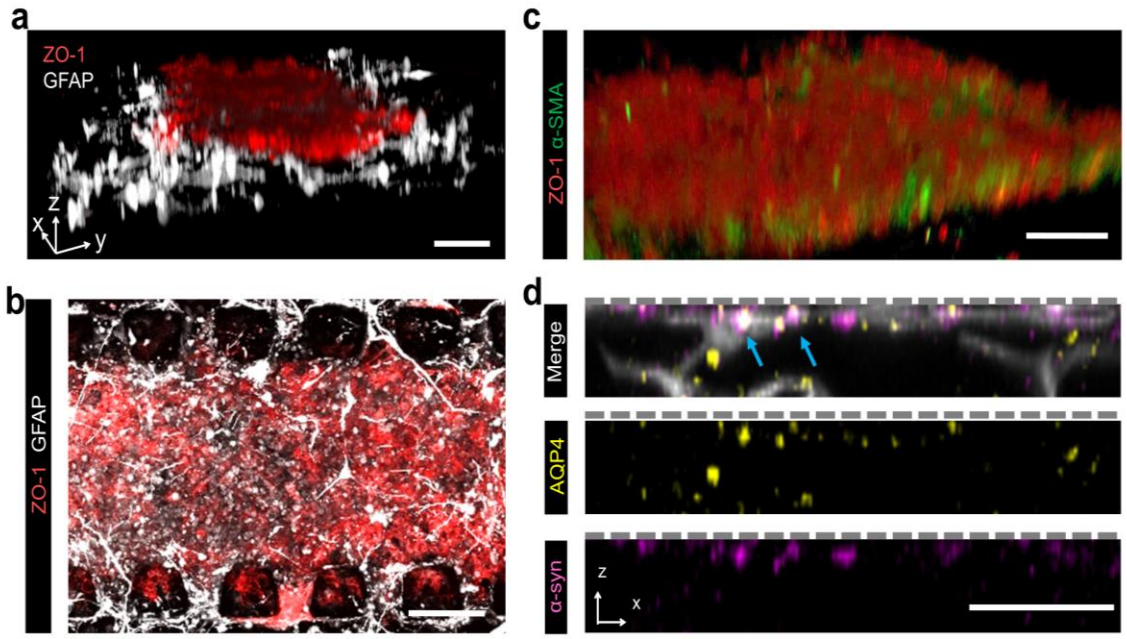

Figure 3.1 Cellular network in microengineered human BBB model. a, 3D configuration of the BBB model showing human brain microvascular endothelial cells (HBMECs) (ZO-1, red) and human astrocytes (HAs) (GFAP, white) (scale bar = 100 μm). **b,** Bottom view of the device with endothelial monolayer (ZO-1, red) and astrocytic network (GFAP, white) (scale bar = 50 μm). **c,** Endothelial monolayer (ZO-1, red) supported by a layer of HBVPs (α-SMA, green) (scale bar = 50 μm). **d,** Aquaporin-4 (AQP4, yellow) and α-syntrophin (α-syn, magenta) expressions at astrocytic end-feet (GFAP, white) underneath a porous membrane (indicated as the dotted line) in the lower channel (Blue arrows indicate co-localization of AQP4 with α-syn.) (scale bar = 50 μm).

3.2.2 Strict endothelial barrier with low permeability

In our BBB chip, HBMECs cultured in the vascular channel under a physiological shear stress (4 dyne/cm^2)[72] establish an intact monolayer with tight junctions (Figure 3.2a) while HBVPs are cultured on the other side of the porous membrane in the perivascular channel (Figure 3.2b,c). Permeability to 4 kDa and 40 kDa FITC-dextran measured for the HBMECs in the presence of the BBB cells (HBVPs and HAs) was significantly lower than that of the monocultured HBMECs, which confirms the tightness of the barrier in our microengineered BBB system (Figure 3.3a). Moreover, our model showed size-dependent molecular transport across the BBB (Figure 3.3a). The TEER values and permeability were comparable to previous BBB studies (Figure 3.3b and Table 3.1).[38,42,85] The permeability coefficient reached as low as the values measured *in vivo*.[88] A physiological level of shear stress was responsible for enhancing barrier tightness increased TEER (Figure 3.3c).

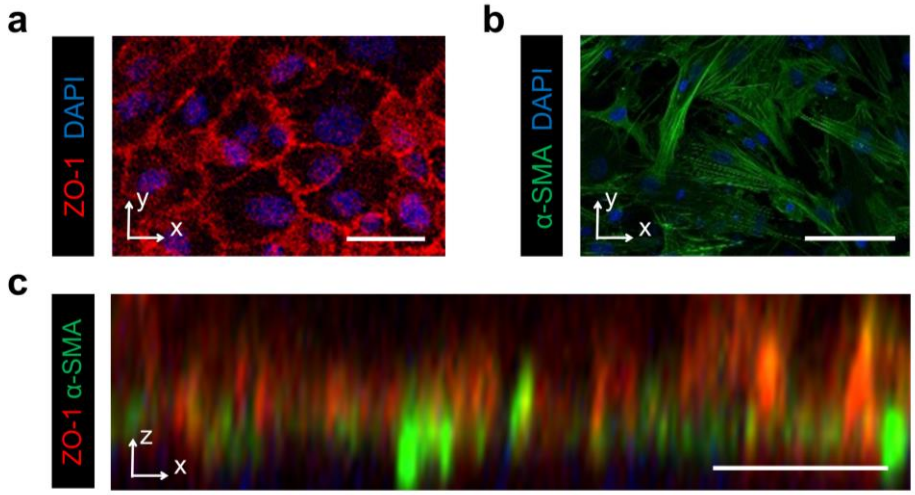

Figure 3.2 Brain endothelium and pericytes cultured on the opposite side of a porous membrane. a, Tight endothelial monolayer (ZO-1, red; DAPI, blue) formed in the upper channel of the device. **b,** Pericytes cultured underneath the porous membrane where an endothelial monolayer is constructed on the other side (α-SMA, green; DAPI, blue). **c**, Bi-layer of endothelial monolayer (ZO-1, red) and HBVPs (α-SMA, green). All scale bars = 50 μm.

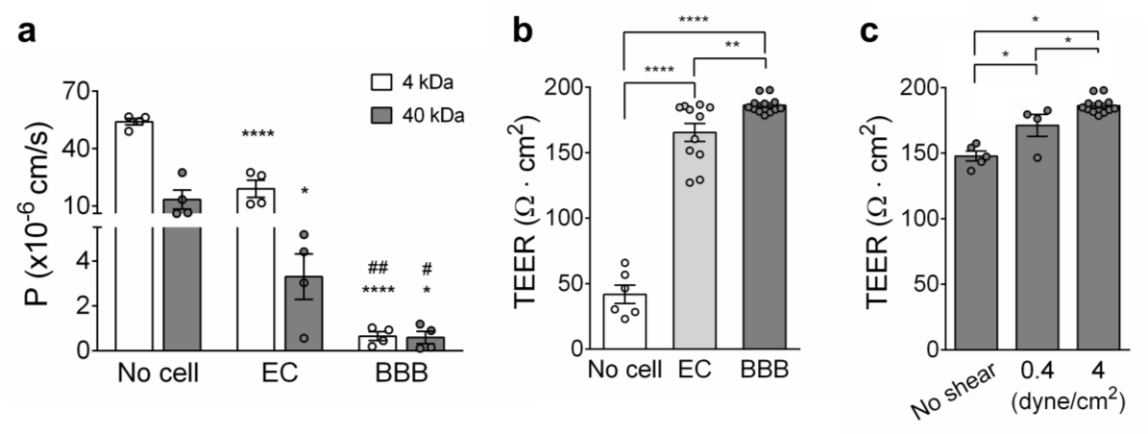

Figure 3.3 Barrier integrity of the endothelial monolayer in the BBB chip. a, TEER measured across the membrane between the upper and lower layers without cells (No cell), with an endothelial monolayer (EC), and an endothelial monolayer with pericytes and astrocytes (BBB) (n=6 for No cell – hydrogel only, n=12 for EC and BBB, **p<0.01 and ****p<0.001). **b,** TEER measured from BBB models under different levels of shear stress (n=5 for No shear, n=4 for 0.4 dyne/cm^2, and n= 12 for 4 dyne/cm^2, *p<0.05) **c,** Permeability coefficients calculated from the diffusion of 4 kDa and 40 kDa FITC-dextran through a membrane (No cell), an endothelial monolayer (EC), an endothelial monolayer co-cultured with pericytes and astrocytes (BBB) (n=4 for each condition, *p<0.05 and ****p<0.001 vs. No cell, #p<0.05 and ##p<0.01 vs. EC).

Table 3.1 Permeability coefficients of current and previous BBB models.

Refs	EC only	BBB	Molecule
This model	1.8E-5	6.5E-7	4kDa FITC dextran
	3.3E-6	5.9E-7	40 kDa FITC dextran
Booth and Kim, Lab Chip., 2012	5E-6	3.5E-6	4kDa FITC-dextran
Adriani et al., Lab Chip., 2017	1.2E-5	3E-5	10kDa FITC-dextran
Wang et al., Mol Pharm., 2016	3.6E-5	6E-7	[^{14}C]-mannitol (182 Da)
Bang et al., Sci.Rep., 2017	1.7E-5	6E-7	20kDa FITC-dextran
Campisi et al., Biomat., 2018	2.2E-6	5E-7	10kDa FITC-dextran
Maoz et al., Nat Biotech., 2018	N/A	2.7E-7	BSA-555 (67kDa)

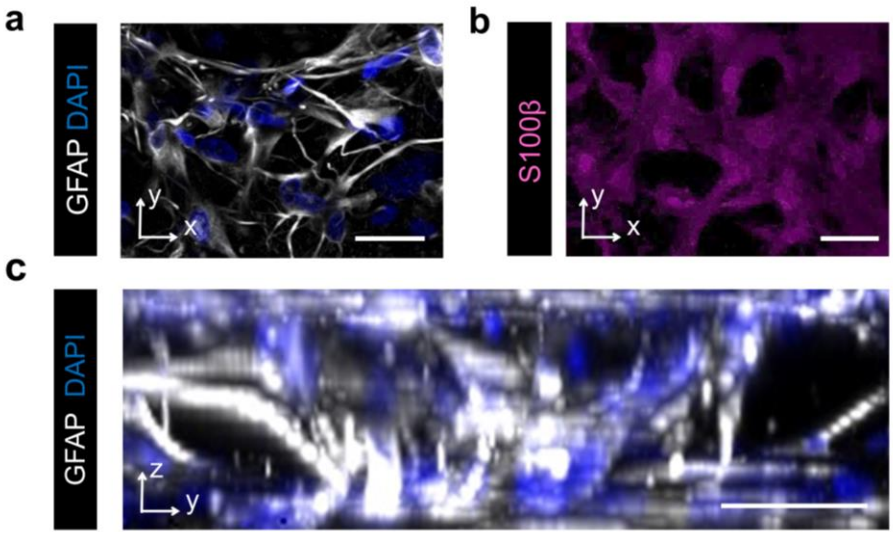

Figure 3.4 3D network of astrocytes in the perivascular channel. a,b, Astrocytes with star-shaped morphology labeled with GFAP (GFAP, white) (**a**) and S100β (S100β, magenta) **(b). c**, Astrocytic end-feet stretching to the endothelium in 3D cellular network (GFAP, white; DAPI, blue). All scale bars = 50 μm.

3.2.3 3D network of astrocyte in a perivascular space

More importantly, HAs cultured in Matrigel of the perivascular channel exhibited a typical star-shaped morphology with radial distribution of fine branches and their 3D cellular network. As previously reported, [89,90] we noted that S100β labels the cytoplasm

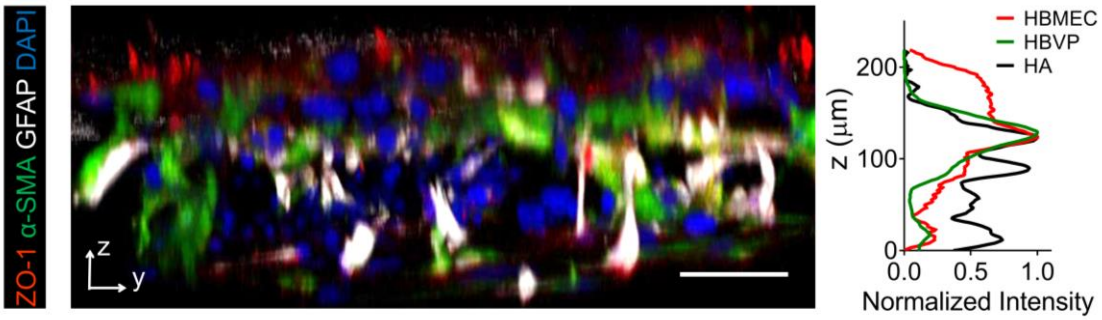

Figure 3.5 3D BBB structure constructed in a device (ZO-1, red; α-SMA, green; GFAP, white; DAPI, blue). The fluorescence intensity profiles indicate the distribution of ZO-1, α-SMA, and GFAP in the image (scale bar = 50 μm).

and nuclei of astrocytes, whereas GFAP labels the cytoplasm and processes (Figure 3.4a,b). HAs created complex 3D network with their branches stretching to the endothelium formed in the vascular channel (Figure 3.4c). This 3D cellular structure in our BBB chip allows for the highly complex yet organized BBB construction (Figure 3.5).

3.2.4 Polarized distribution of aquaporin-4 in the BBB chip

Astrocytes in the perivascular space play a role in regulating the water homeostasis in the brain via the water channel protein AQP4 at their end-feet processes.[20,21] Localization of AQP4 in astrocytic end-feet processes is therefore important to recapitulate the BBB in homeostatic and physiological conditions. Our BBB model recapitulates a complex 3D network of HAs with expression of AQP4 along their branches while 2D culture models show diffusively expressed AQP4 in plasma membrane of astrocytes **(**Figure S 3.3**).** We analyzed AQP polarization by calculating the ratio of AQP4 labelled along astrocytic end-feet in a vascular side versus that in a parenchymal side of the perivascular channel as previously reported[14] (Figure 3.6a) and by demonstrating co-localization with α-syntrophin, the immediate anchor for AQP4

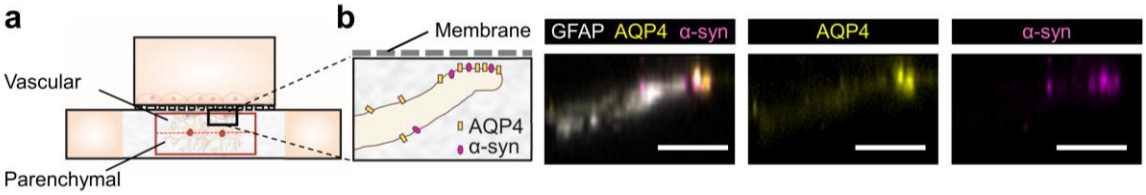

Figure 3.6 Astrocytic end-feet underneath a porous membrane. a, Schematic showing the location of astrocytic end-feet with Aquaporin-4 (AQP4) and α-syntrophin (α-syn) colocalization. **b,** Co-localization of AQP4 (AQP4, yellow) and α-syntrophin (α-syn, magenta) at astrocytic end-feet (scale bars = 20 μm).

that controls AQP4 polarization to astrocytic end-feet, in the model (Figure 3.6b). The localization of AQP4 in HAs was polarized to the astrocytic end-feet in the vascular side of the channel when cultured with HBMECs and HBVPs (Figure 3.7a-c). The polarized distribution of AQP4 was significantly induced in the presense of HBVPs, as previously observed *in vivo*.[10] This finding implies that our model can mimic the water transport system at the BBB, which is responsible for the homeostasis of ions and water in the brain.

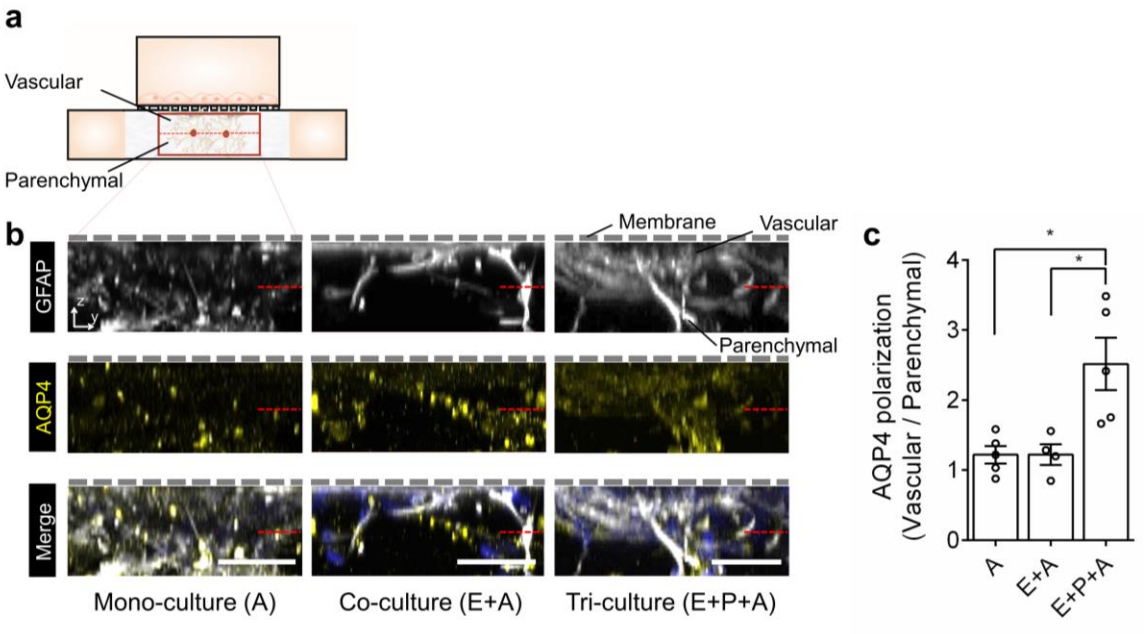

Figure 3.7 Polarized distribution of aquaporin-4 in the BBB chip. a, Quantitative analysis of AQP4 polarization by measuring AQP4 distribution in vascular and parenchymal side in the perivascular channel. **b,** Distribution of AQP4 (AQP4, yellow) along the cell bodies of HAs (GFAP, white; DAPI, blue) in the channel (scale bars = 50 μm). **c,** Polarized expression of AQP4 to the vascular side in the perivascular channel (n=4 for each condition, *p<0.05).

3.3 Conclusions

Our on-chip human BBB model successfully recapitulated the key structure and function of the BBB featuring the highly specialized brain endothelial monolayer and physiological network of astrocytes. The new hybrid design combining two vertical layers with three parallel channels enabled the complex BBB co-culture with high reproducibility, not only establishing a 2D intact brain endothelium and reconstructing a 3D brain microenvironment with astrocytic network but also connecting the BBB cells in perfusable proximity for their intercellular signaling in co-culture. Moreover, the present BBB model is the first of its kind to show the polarized distribution of AQP4 in perivascular astrocytes, which is critical to mimic the BBB physiology that maintains water and ion homeostasis in the brain. AQP4 is also involved in brain pathophysiology including glial scar formation[22] and neuroinflammation[23]. Taken together, our model established the physiologically relevant human BBB with the ability to control status of astrocytes from resting to reactive conditions as a potential for modeling of neuroinflammation and reactive gliosis in CNS diseases.

3.4 Materials and Methods

Fabrication of the microfluidic device. The microfluidic device was fabricated with polydimethylsiloxane (PDMS; Sylgard 184; Dow Corning, Midland, MI, USA) using soft lithography.[79] To create the PDMS slab for the upper layer, PDMS pre-polymer (10:1 elastomer base to curing agent, wt/wt) was degassed and poured onto silicon wafers patterned with SU-8 (Microchem, Newton, MA, USA). The thin PDMS sheet for the lower

layer of the device was created by spin coating an SU-8 patterned silicon wafer with a PDMS pre-polymer to a height of 250 μm. After curing the PDMS pre-polymer for 1 h at 80˚C, inlets and outlets of the channels were formed with 1 mm diameter biopsy punch. A polycarbonate membrane (8 μm pore; Sterlitech Corp, Kent, WA, USA) treated with 5% 3-aminopropyl-trienthoxysilane (APTES) solution (Sigma-Aldrich, St. Louis, MO, USA)[80] was sandwiched and bonded between the upper and lower PDMS layers using a plasma cleaner (Harrick Plasma, Ithaca, NY, USA). The fabricated device was then placed in a polystyrene box (Ted Pella Inc., Redding, CA, USA). The device and microchannels are sterilized with 70% ethanol and placed in a dry oven at 80˚C for 2.5 days to restore hydrophobicity of the PDMS surface.

Cell culture. Immortalized human brain microvascular endothelial cells (HBMEC; Innoprot, Bizkaia, Spain) at passage 5-10 were maintained in endothelial cell medium (Sciencell, San Diego, CA, USA) on flasks coated with 50 μg/mL fibronectin (Sigma Aldrich). Human brain vascular pericytes (HBVP) and human astrocytes (HA) (Sciencell) were cultured on 1 mg/mL poly-l-lysine (PLL, Sigma Aldrich) coated flasks and maintained in astrocyte and pericyte medium, respectively (Sciencell). Both primary cells between passages 3 and 5 were used for all experiments. Fibronectin and PLL coating procedures were achieved following the manufacturer's instruction.

Construction of the BBB chip system. Prior to seeding HBVPs into the center channel of the lower layer, the channel was coated with 50 μg/mL fibronectin (Sigma-Aldrich) for 1 h at 37 ˚C while the device was placed upside down. Then HBVPs were seeded at 1 x 10^7 cells/mL density into the center channel and incubate for 6 h to allow adhesion of cells onto the fibronectin-coated polycarbonate membrane. Then 1 x 10^7 HAs suspended in a

100 μL of Matrigel solution (Growth factor-reduced; Corning, Corning, NY, USA) were seeded into the same channel that HBVPs are cultured. The final concentration of Matrigel was calculated to be 5 mg/mL. After gelation of Matrigel in the channel by incubating at 37˚C for 30 min, cell culture medium was filled into the two side channels to avoid the gel drying out. The device was placed in the incubator at 37 ˚C for 6 h, and the upper luminal channel of the device was coated with 50 μg/mL fibronectin for 1 h at 37 ˚C. HBMECs were then seeded into the upper channel with the density of 7 x 10^7 cells/mL. The final cell number ratio between HBMECs and HBVPs in a device was 1.5:1, and the ratio between HBMECs and HAs was 2:1, which was optimized for HAs to cover ~99% of the perivascular surface of the endothelium. After 24 h of culture to stabilize cells in the microfluidic device, the upper channels were connected to PhD Ultra syringe pumps (Harvard Apparatus, Holliston, MA, USA) and exposed to the media flow with the flow rate of 16 μL/min to give cells the shear stress of 4 dyne/cm^2, which corresponds to the shear stress levels in the brain.[72]

Immunocytochemistry. To visualize cell-specific marker expression, immunocytochemistry was performed. Briefly, samples were fixed with 2% paraformaldehyde (PFA; Santa Cruz Biotechnology, San Diego, CA, USA) for 15 min at RT. After permeabilizing in 0.1% Triton X (Sigma-Aldrich) in PBS for 15 min, the samples were blocked with 2% bovine serum albumin (BSA; Sigma-Aldrich) in PBS for 1 h at RT. Subsequently, the samples were incubated with primary antibodies at 4 ˚C overnight, washed three times with 1% BSA. The following antibodies were used for immunocytochemistry: mouse anti-GFAP (1:200; Invitrogen, Carlsbad, CA, USA), rabbit anti-S100β (1:200; Invitrogen), and rabbit anti-AQP4 (1:200; Invitrogen). Then samples

were incubated with fluorescence-conjugated secondary antibodies (chicken anti-mouse AlexaFluor 594) (1:200; Invitrogen) for 6 h at 4 ˚C to visualize targets. Nuclei were counterstained with 4,6-diamino-2-phenylindole (DAPI; Invitrogen) and stored in PBS before imaging. Fluorescently visualized samples were examined using a confocal microscope (LSM 700, Carl Zeiss, Oberkochen, Germany).

Permeability measurement. After 60 h of culture, culture medium containing 500 μg/mL of 4 kDa or 40 kDa FITC-dextran (Sigma-Aldrich) was introduced into the luminal channel of the device at 16 μL/min with a PhD Ultra syringe pump (Harvard Apparatus). Simultaneously, culture medium from one side channel was sampled at 4 μL/min with a syringe pump for 1 h. Fluorescence intensities of 500 μg/mL of FITC-dextran solution and the sampled solutions are measured using a Cytation 5 plate reader (n=4 for each condition). The dextran concentrations in the solutions were calculated with the measured fluorescence intensity values using a standard calibration curve. Permeability coefficients were calculated using the following equation:

$$P = V\frac{\frac{dC}{dt}}{\Delta C}$$

Where V is the volume of the sampled solution, A is the surface area of the endothelial barrier, $\frac{dC}{dt}$ is the concentration change in the abluminal space along time, and ΔC is the concentration difference across the barrier.

TEER measurement. The TEER of the endothelial monolayer formed in the device was measured using Ag/AgCl electrode wires (381 μm in diameter and 3 cm in length, A-M Systems, Sequim, WA, USA) connected to EVOM2 volt-ohmmeter (Word Precision

Instruments, Sarasota, FL, USA) which generates a constant 10 μA of AC current at 12.5 Hz while measuring resistance. To reduce background resistance and error, the electrode wires were placed in a tygon tubing (1/32"ID x 3/32"OD, Cole-Parmer, Vernon Hills, IL, USA) filled with culture medium and inserted into the channels. After 1 min of stabilization, 5 multiple readings were averaged for each device. To calculate TEER, the measured resistance was multiplied by the surface area of endothelial monolayer overlapping with the lower channel (0.015 cm^2).

Image analysis. Quantitative analysis of cell distribution and aquaporin-4 polarization were performed using ImageJ (NIH, Bethesda, MD, USA). For cell distribution analysis, fluorescence intensity profile of each color (red, green, and white) was analyzed using Matlab (Mathworks, Natick, MA, USA). Distribution of AQP4 was quantified by measuring the fluorescence intensity profile along the z-axis in z-stack images of the perivascular channel using ImageJ. The lower channel was divided into the two spaces (top half – vascular side, bottom half – parenchymal side) and the average of the fluorescence intensity from each space was calculated. The averaged intensity within the top half space (vascular side) was divided by the averaged normalized intensity within the bottom half space (parenchymal side) to calculate the AQP4 polarization index.

3.5 Supplementary Information

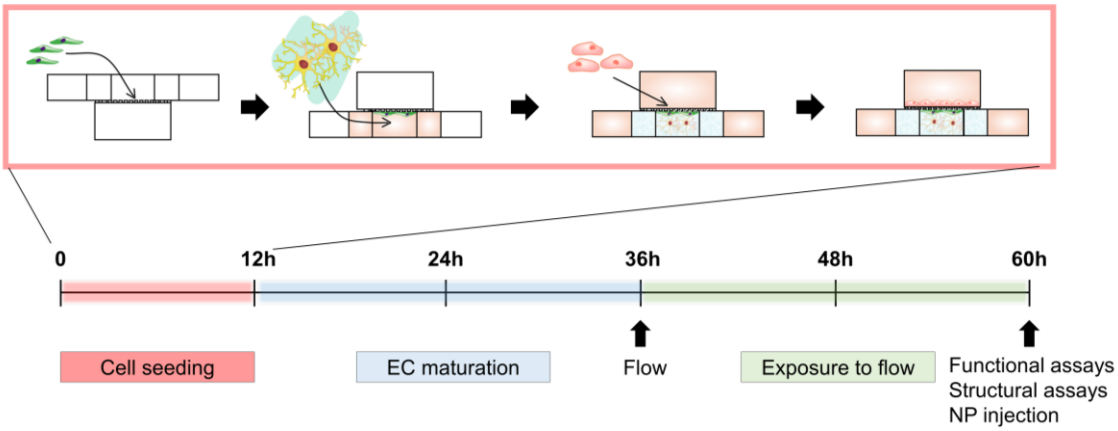

Figure S 3.1 Timeline of the experiments. The procedure for cell seeding into the device is as follows: 1. Culture HBVPs on a porous membrane in the abluminal region, while the device is flipped. 2. Inject a glial cells-embedded hydrogel in the abluminal center channel. 3. After 12 hours, culture HBMECs on a porous membrane in the luminal side for additional 1 day. 4. Apply shear flow into the luminal channel for 1 day to establish a tightly connected monolayer.

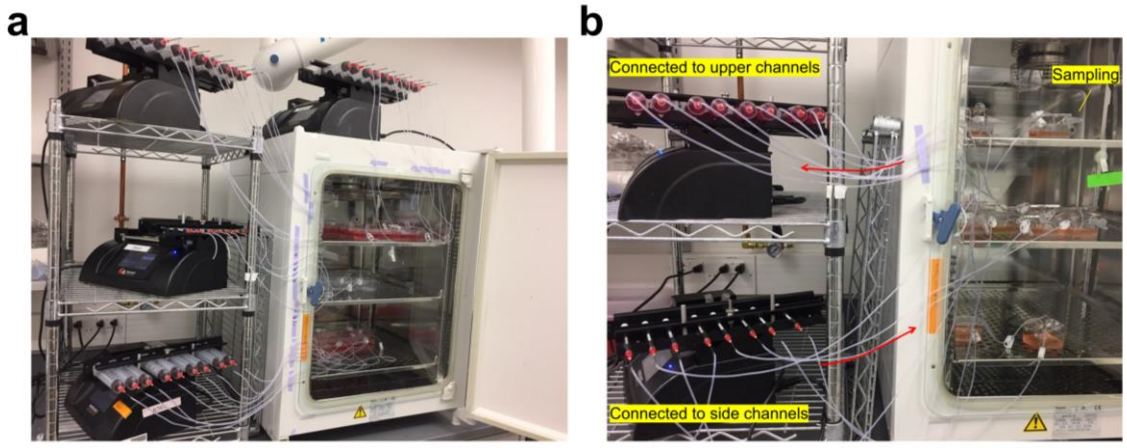

Figure S 3.2 High-throughput experimental setup. a, High-throughput experimental setup using multi syringe racks. **b,** Experimental setup for permeability assay and molecular sampling.

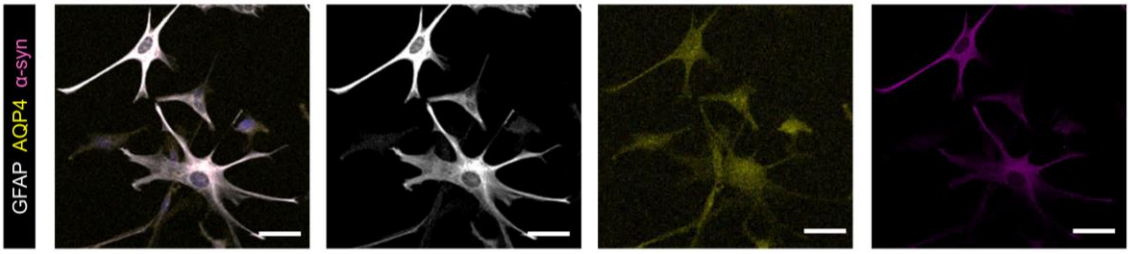

Figure S 3.3 Aquaporin-4 (AQP4) and α-syntrophin (α-syn) expression in 2D cultured astrocytes. Confocal images of 2D monoculture of astrocytes (GFAP, white) showing diffusive expression of AQP4 (AQP4, yellow) and α-syn (α-syn, magenta). Scale bars = 50 µm.

CHAPTER 4. EVALUATION OF NANOPARTICLE TRANSPORT AND DISTRIBUTION ON A BBB MODEL

4.1 Introduction

Many potential drugs for the central nervous system (CNS) diseases fail in clinical trials mainly due to a unique CNS barrier structure, the blood-brain barrier (BBB).[1] To deliver drugs across this barrier, CNS delivery systems have been widely explored to cross the BBB,[91] including nanoparticle (NP)-mediated drug delivery with ligands specific to BBB endothelial surface receptors.[46,47] In particular, high-density lipoprotein (HDL)-mimetic NPs have been introduced as promising CNS delivery systems due to the innate endogenous character to facilitate the delivery of therapeutic molecules across the BBB via lipoprotein receptor-mediated transcytosis.[56,61,62] However, the lack of experimental models that can precisely evaluate the interactions between the BBB and delivery carriers restricts successful clinical translation of therapeutic and diagnostic NPs.[24,25] Animal models often do not predict drug responses in humans due to species differences.[26,63,64] Moreover, the complex physiology of animal models makes it difficult to perform mechanistic studies and direct quantitative analysis of NPs with the barrier at molecular and cellular levels in real time.[24] These challenges highlight the importance of developing an *in vitro* model that mimics the essential physiological structure and function of the human BBB and that reproduces the key relationships of healthy and disrupted barrier functions in a controlled manner. Moreover, effective experimental strategies that can quantitatively analyze the NP transport, distribution, and delivery to targeted cells or regions will enable robust preclinical screening of the NPs.

In this study, we use our microengineered human BBB model to assess NP transport and distribution at the BBB. The model combined with high-precision sampling and flow cytometric analysis enables on-chip quantification of nanoparticle transport and distribution in the vascular and perivascular regions at cellular and tissue levels. Our BBB chip may provide a reliable tool for better understanding of drug distribution and efficacy at the BBB in both physiological and pathological conditions.

4.2 Results and Discussions

4.2.1 Microfluidic synthesis of the biomimetic nanoparticle

We synthesized a bioinspired nanoparticle that mimics the natural high-density lipoproteins (HDL) in our body, which have high stability and long circulation time. Moreover, these HDL particles are known to be able to translocate the BBB via lipoprotein receptors expressed at the brain endothelium such as scavenger receptor type B1 (SR-B1) (Figure 4.1a).[46,56,92] Thus, the HDL-mimetic particles that can reconstitute the innate ability of the plasma HDL is a promising drug carrier for CNS drug delivery.

We used our microfluidic technology to engineer HDL-mimetic nanoparticles with apolipoprotein A1 (eHNP-A1) (Figure 4.1b). The microfluidic synthesis increased the efficiency of mixing the precursor solutions while decreased the number of formulation steps, resulting in high yield and homogeneity of the eHNP-A1. The eHNP-A1 showed discoidal structure and the physiologically relevant size with a diameter of

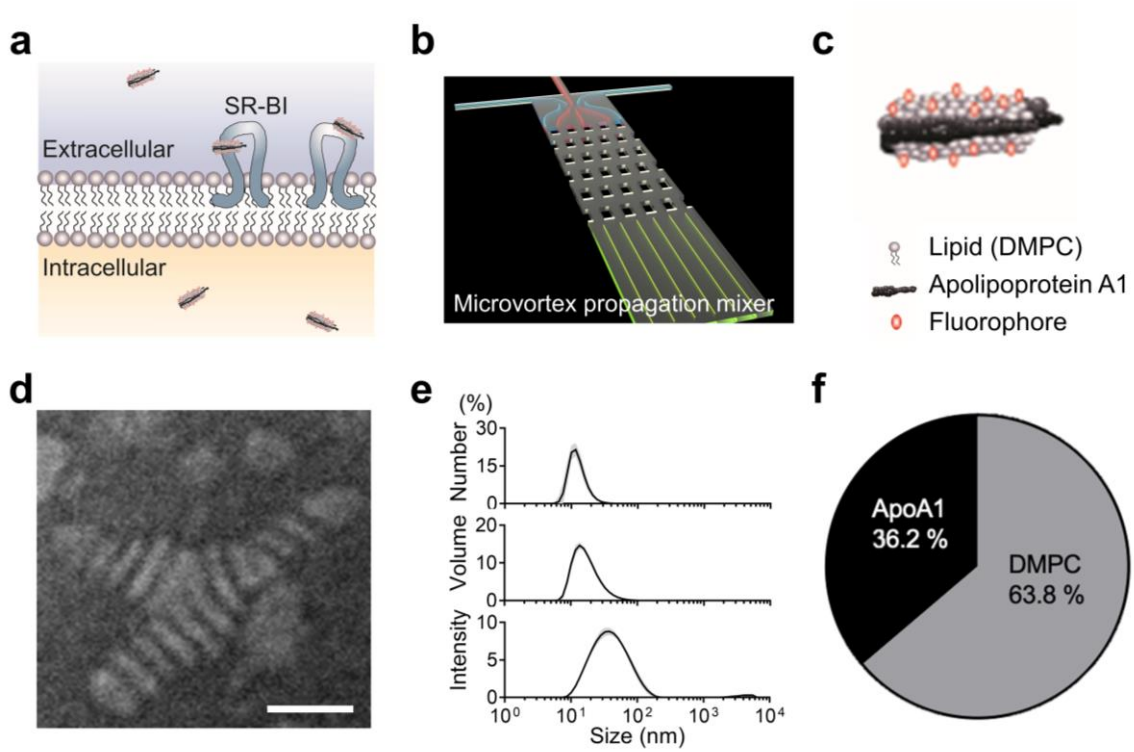

Figure 4.1 The engineered high-density lipoprotein mimicking nanoparticle with apolipoprotein-A1 (eHNP-A1). a, Schematic description of scavenger receptor type B1 (SR-B1) mediated eHNP-A1 transcytosis. **b,** Schematic description of eHNP-A1 synthesis using the microvortex propagation mixer (μVPM). **c,** Discoidal eHNP-A1 consisting of lipid, apolipoprotein A1, and fluorescent marker. **d,** Transmission electron microscopy (TEM) image of the synthesized eHNP-A1 (scale bar=20 nm). **e,** Size distribution of the synthesized eHNP-A1. **f,** Composition of the eHNP-A1.

10-20 nm (Figure 4.1c-e). Moreover, the microfluidic synthesis resulted in high reproducibility and unform sizes and composition of the eHNP-A1(Figure 4.1f).

4.2.2 Brain accumulation of the biomimetic nanoparticle

We confirmed through a biodistribution study following intravenous injection of the fluorescent-dye labeled eHNP-A1s that eHNP-A1 can enter the BBB with approximately 3% of relative accumulation in the brain (Figure 4.2a,b and Figure S

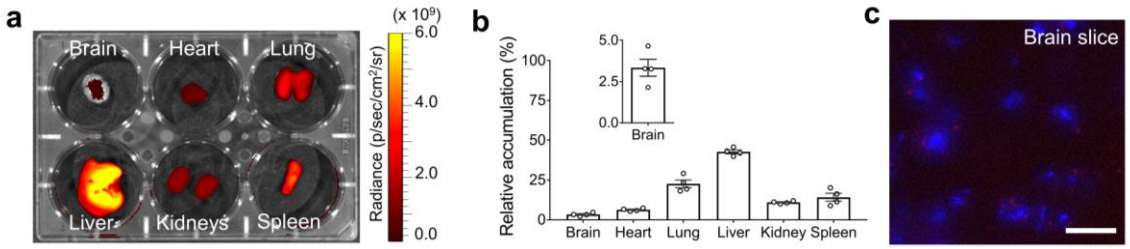

Figure 4.2 Biodistribution of the eHNP-A1. a, Biodistribution of the eHNP-A1. **b**, Quantification of the relative fluorescence intensity in each organ (n=4 for each condition). **c**, eHNP-A1 accumulated in the mouse brain (scale bar=50 μm).

4.1). Such brain delivery efficiency is higher than that of other well-known NPs for brain targeting drug delivery,[48] possibly due to the interaction with receptors on brain ECs. Confocal imaging analysis of the cryosectioned brain tissue confirmed that the systemically administered eHNP-A1s were localized around the cell nucleus (Figure 4.2c). Further examination of the eHNP-A1 distribution in vascular and perivascular regions or in different cell types at the BBB can be done with the BBB chip.

4.2.3 Nanoparticle transport analysis on chip

One challenge in CNS drug delivery research is to accurately quantify the transport of drug compounds into the brain at cellular and molecular levels. Our BBB chip allows for the monitoring of the interactions between cells and NPs but also enables us to quantify the distribution of NPs in vascular and perivascular spaces as well as in each cell type.

We quantified eHNP-A1 distributions in the vascular and perivascular spaces at the BBB and studied the transport mechanisms in a controlled manner. We hypothesized that when a NP solution is introduced into our BBB chip, NPs either

remain in the vascular channel, interact with HBMECs, or translocate into the perivascular channel in which NPs can interact with HBVPs or HAs (Figure 4.3a-c). With the results of eHNP-A1's BBB penetration as shown in our animal study (Figure 4.2), we used our BBB chip to investigate the mechanism by which eHNP-A1 can get into the brain. We tested the hypothesis that eHNP-A1 primarily leverages scavenger receptor class B type 1 (SR-B1) on brain endothelial cells to cross the BBB via transcytosis, one of the major transport mechanisms of natural HDL.[93,94] After blocking SR-B1, the amount of eHNP-A1 remaining in the vascular channel significantly increased (Figure 4.3d), whereas the amount of eHNP-A1 translocated to the perivascular channel was not significantly changed (Figure 4.3e). This result indicates that blocking SR-B1 activity reduces eHNP-A1 uptake by HBMECs, whereas it may induce a compensatory upregulation of other receptors or determinants of endothelial transcytosis such as SNAREs.[93,95] We then mapped the 3D distribution of eHNP-A1 in our BBB chip by compensating NP loss caused by the adsorption to the PDMS surface (Figure S 4.2). Our results revealed that block lipid transport-1 (BLT-1) treatment reduced the amount of eHNP-A1 that gets into the tissue ("EC uptake" and "perivascular channel") by ~3 fold (Figure 4.3f,g). Cellular uptake of eHNP-A1 was further quantified using Fluorescence-activated cell sorting (FACS) analysis. The total portion of eHNP-A1 positive cells was decreased in the BLT-1 treated BBB models (Figure 4.3h,i), indicating that SR-B1 mediates the cellular uptake of eHNP-A1 in our BBB chip as shown in previous study.[93] In particular, the portion of perivascular cells (i.e. HBVPs and HAs) that have taken up eHNP-A1 was decreased by 38.5% and 53.8% respectively

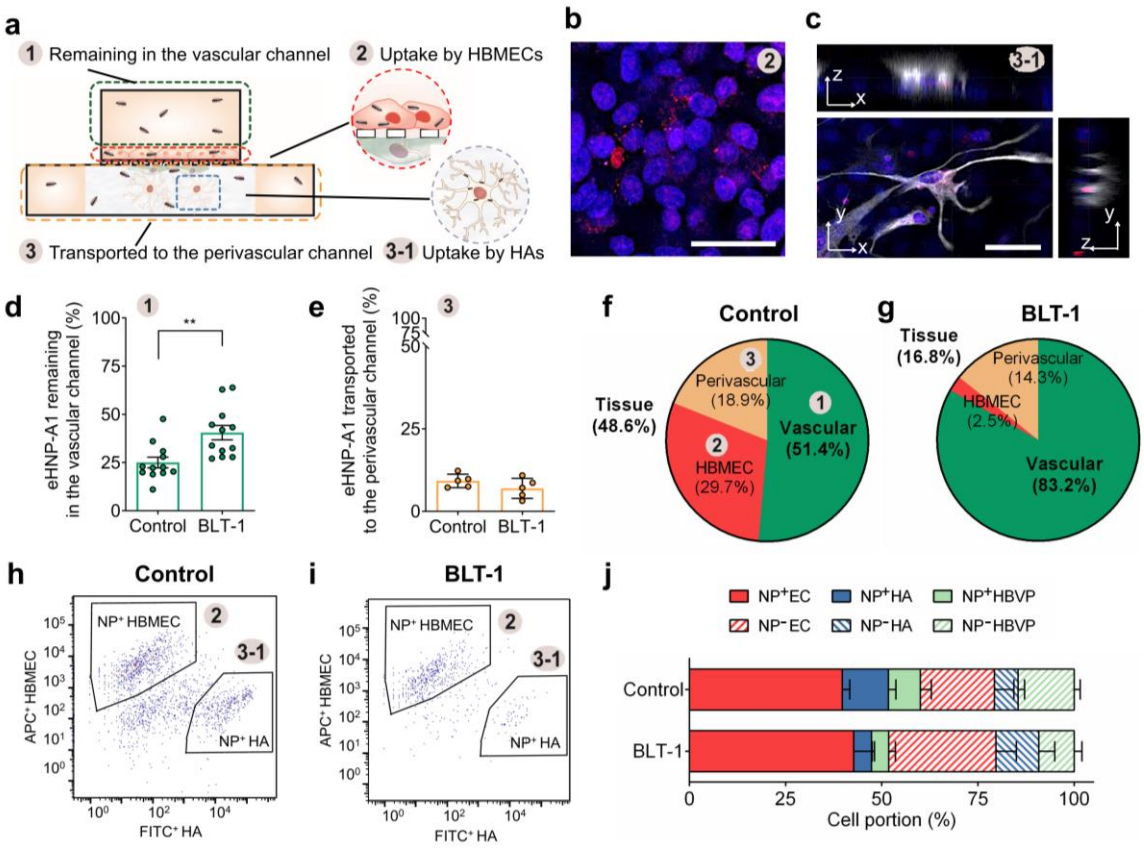

Figure 4.3 Distribution of the eHNP-A1 in the BBB model. a, Schematic description of eHNP-A1 distribution in the BBB model showing (1) eHNP-A1 remaining in the vascular channel, (2) eHNP-A1 interact with endothelial cells (HBMECs), (3) eHNP-A1 translocated to the perivascular channel, and (3-1) eHNP-A1 interact with astrocytes (HAs). **b,c,** Confocal images showing eHNP-A1s within the HBMEC monolayer (**b**) and HAs (**c**) in a BBB chip (scale basr=50 μm). **d,e,** Relative fluorescence intensity of sampled culture medium containing eHNP-A1 from the upper channel (**d**) and the lower channel (**e**) after 2 hours of eHNP-A1 incubation in the vascular channel (k: n=12; l: n=5, **p<0.01). **f,g,** Distribution of eHNP-A1 in control (**f**) and the BLT-1 treated microengineered BBB model (**g**). **h,i,** Representative Fluorescence-activated cell sorting (FACS) plot for the numbers of eHNP-A1 positive HBMECs and HAs in control (**h**) and BLT-1 treated BBB models (**i**). **j**, Cellular uptake of eHNP-A1 in the BBB chip quantified from FACS analysis (n=3)**.**

with BLT-1 treatment, whereas the portion of HBMECs with eHNP-A1 was not changed (Figure 4.3j).

4.3 Conclusions

The brain-blood ratio of a drug concentration, a key parameter to estimate brain pharmacokinetics and brain-targeting efficiency, has been previously assessed using rodents by *in situ* brain perfusion, brain microdialysis, and neuropharmacokinetic study.[96,97] Given the complexity of the techniques and species differences between humans and rodents, there is a critical need for new strategies that quickly and reliably measure how much drugs can penetrate to the brain parenchyma in a dose-dependent manner at multiple time points.[98] Our BBB model integrated with precise time-lapse sampling and end-point FACS analysis allowed us to precisely quantify 3D nanoparticle distribution at the BBB. Compartmentalized structure of the BBB chip conferred the ability to measure the amount of molecules separately for each space, allowing for quantitative assessment of BBB penetrations. Quantitative analysis of cellular uptakes in the BBB chip enabled us to evaluate the targeting efficacy of nanoparticles at cellular levels. Moreover, our model provided an in depth mechanistic understanding of the interactions between the BBB and nanoparticles at cellular levels.

In summary, to assess NP transport across the BBB, we used a HDL-mimetic NP synthesized with our microfluidic technology, which we recently reported.[99] Using our BBB chip, we demonstrated that eHNP-A1 is a potential CNS drug delivery system with their biomimetic ability to cross the BBB via SR-B1 mediated transcytosis. Our novel approach to 3D mapping of nanoparticle distributions in the vascular and perivascular spaces at the BBB will impact drug delivery and organs-on-chips areas.

4.4 Materials and Methods

Fabrication of the microfluidic device. The microfluidic device was fabricated with polydimethylsiloxane (PDMS; Sylgard 184; Dow Corning, Midland, MI, USA) using soft lithography.[79] To create the PDMS slab for the upper layer, PDMS pre-polymer (10:1 elastomer base to curing agent, wt/wt) was degassed and poured onto silicon wafers patterned with SU-8 (Microchem, Newton, MA, USA). The thin PDMS sheet for the lower layer of the device was created by spin coating an SU-8 patterned silicon wafer with a PDMS pre-polymer to a height of 250 µm. After curing the PDMS pre-polymer for 1 h at 80˚C, inlets and outlets of the channels were formed with 1 mm diameter biopsy punch. A polycarbonate membrane (8 µm pore; Sterlitech Corp, Kent, WA, USA) treated with 5% 3-aminopropyl-trienthoxysilane (APTES) solution (Sigma-Aldrich, St. Louis, MO, USA)[80] was sandwiched and bonded between the upper and lower PDMS layers using a plasma cleaner (Harrick Plasma, Ithaca, NY, USA). The fabricated device was then placed in a polystyrene box (Ted Pella Inc., Redding, CA, USA). The device and microchannels are sterilized with 70% ethanol and placed in a dry oven at 80˚C for 2.5 days to restore hydrophobicity of the PDMS surface.

Cell culture. Immortalized human brain microvascular endothelial cells (HBMEC; Innoprot, Bizkaia, Spain) at passage 5-10 were maintained in endothelial cell medium (Sciencell, San Diego, CA, USA) on flasks coated with 50 µg/mL fibronectin (Sigma Aldrich). Human brain vascular pericytes (HBVP) and human astrocytes (HA) (Sciencell) were cultured on 1 mg/mL poly-l-lysine (PLL, Sigma Aldrich) coated flasks and maintained in astrocyte and pericyte medium, respectively (Sciencell). Both primary cells

between passages 3 and 5 were used for all experiments. Fibronectin and PLL coating procedures were achieved following the manufacturer's instruction.

Construction of the BBB chip system. Prior to seeding HBVPs into the center channel of the lower layer, the channel was coated with 50 μg/mL fibronectin (Sigma-Aldrich) for 1 h at 37 ˚C while the device was placed upside down. Then HBVPs were seeded at 1 x 10^7 cells/mL density into the center channel and incubate for 6 h to allow adhesion of cells onto the fibronectin-coated polycarbonate membrane. Then 1 x 10^7 HAs suspended in a 100 μL of Matrigel solution (Growth factor-reduced; Corning, Corning, NY, USA) were seeded into the same channel that HBVPs are cultured. The final concentration of Matrigel was calculated to be 5 mg/mL. After gelation of Matrigel in the channel by incubating at 37˚C for 30 min, cell culture medium was filled into the two side channels to avoid the gel drying out. The device was placed in the incubator at 37 ˚C for 6 h, and the upper luminal channel of the device was coated with 50 μg/mL fibronectin for 1 h at 37 ˚C. HBMECs were then seeded into the upper channel with the density of 7 x 10^7 cells/mL. The final cell number ratio between HBMECs and HBVPs in a device was 1.5:1, and the ratio between HBMECs and HAs was 2:1, which was optimized for HAs to cover ~99% of the perivascular surface of the endothelium. After 24 h of culture to stabilize cells in the microfluidic device, the upper channels were connected to PhD Ultra syringe pumps (Harvard Apparatus, Holliston, MA, USA) and exposed to the media flow with the flow rate of 16 μL/min to give cells the shear stress of 4 dyne/cm^2, which corresponds to the shear stress levels in the brain.[72]

Immunocytochemistry. To visualize cell-specific marker expression, immunocytochemistry was performed. Briefly, samples were fixed with 2%

paraformaldehyde (PFA; Santa Cruz Biotechnology, San Diego, CA, USA) for 15 min at RT. After permeabilizing in 0.1% Triton X (Sigma-Aldrich) in PBS for 15 min, the samples were blocked with 2% bovine serum albumin (BSA; Sigma-Aldrich) in PBS for 1 h at RT. Subsequently, the samples were incubated with primary antibodies at 4 ˚C overnight, washed three times with 1% BSA. Then samples were incubated with fluorescence-conjugated secondary antibody for 6 h at 4 ˚C to visualize targets. The following antibodies were used for immunocytochemistry: mouse anti-GFAP (1:200; Invitrogen, Carlsbad, CA, USA), chicken anti-mouse AlexaFluor 594) (1:200; Invitrogen) Nuclei were counterstained with 4,6-diamino-2-phenylindole (DAPI; Invitrogen) and stored in PBS before imaging. Fluorescently visualized samples were examined using a confocal microscope (LSM 700, Carl Zeiss, Oberkochen, Germany).

Nanoparticle (NP) synthesis. The microvortex propagation mixer (μVPM) that we reported previously[99] was used for the synthesis. Briefly, the μVPM was connected to syringe pumps (Harvard Apparatus) to introduce the solutions into the device. The precursor solutions including a lipid solution that was composed of 1,2-dimyristoyl-sn-glycero-3-phosphocholine (DMPC; Avanti Polar Lipids, Alabaster, AL, USA) with a concentration of 2.75 mg/mL in ethanol, and a Apolipoprotein A1 from human plasma (Sigma-Aldrich) with a concentration of 0.2 mg/mL in PBS were added into the mixer. The flow ratio between the side streams and the center stream in the mixer was 5.5:1. The mixed solution was collected and then washed three times with PBS using a 10,000 M.W. centrifugal filter (EMD Millipore Corp., Darmstadt, Germany) at a speed of 3900 rpm for 20 min. The size distribution of the final sample was measured with a Zetasizer Nano ZS (Malvern Instruments, Worcestershire, United Kingdom). Fluorescently labeled eHNPs

were synthesized with 1,1′-Dioctadecyl-3,3,3′,3′-Tetramethylindotricarbocyanine Iodide (DiR′; Invitrogen) or a modified lipid precursor solution containing 15% (w/w) 1,2-dimyristoyl-sn-glycero-3-phosphoethanolamine-N-(lissamine rhodamine B sulfonyl) (Rhodamine-DMPE; Sigma-Aldrich). The amount of protein of the final sample was quantified using the Micro BCA Protein Assay kit (Invitrogen).

Biodistribution study. All animal experiments were reviewed and approved by the Georgia Tech's Institutional Animal Care and Use Committee. 4-5 week-old male balb/c mice (Jackson Labs, city, state, USA) were given an irradiated dietary regiment until the mice were 21-22 weeks of age. For biodistribution study, 1 mg/kg of eHNP-A1 was systemically administered to the mouse via tail vein injection. Injection of 200 μL saline was served as control. 24 h after administration, mice were sacrificed and perfused with saline and 4% PFA for 15 min. Then organs (brain, heart, lung, liver, kidneys, and spleen) were harvested to visualize their DiR content using an in vivo imaging system (IVIS; Perkin Elmer, Waltham, MA, USA). To visualize the eHNP-A1 internalization inside the brain tissue, the harvested brain tissues were cryosectioned into 10 μm slices and stained with DAPI using the DAPI-containing antifade mounting medium (H-1200; Vector Laboratories, Burlingame, CA). The slides were then imaged under a confocal microscope (Zeiss LSM 780).

Nanoparticle distribution study in a chip. Culture medium containing eHNP-A1 at a concentration of 10 μg/mL was introduced into the upper channel of the device. To block the NP transport via SR-B1, 200 μM of BLT-1 (Sigma Aldrich) was treated in the upper channel for 1 h prior to the NP incubation. Following 2 h of NP incubation with culture medium with or without BLT-1 (200 μM), 10 μL of culture medium was sampled from the

upper channel. The upper channel was washed with PBS and filled with Dispase (Corning) to digest Matrigel in the lower channel. After 30 min, 10 µL of the mixture of the culture medium and digested Matrigel from the lower channels were collected. To measure the concentrations of nanoparticles, fluorescence intensities of the culture medium injected into the upper channel, sampled from the upper channel (n=14 for control and n=13 for BLT-1), and the culture medium sampled from the lower channels (n=7 for control and n=5 for BLT-1) were measured using the Cytation 5 plate reader.

Nanoparticle uptake study using flow cytometric analysis (FACS). Prior to seeding cells into the device, HBMECs and HAs were fluorescently labeled with CellTracker™ (Deep Red and Green CMFDA, respectively; Invitrogen) as per manufacturer's instructions. After 2 h of 10 µg/mL of NP incubation in the upper channel of the device, the devices were washed three times with PBS and 0.25% Trypsin-EDTA (Invitrogen) and Dispase (Corning) were injected into the upper channel and lower side channels, respectively. HBMECs and HAs were then collected in culture medium and spun down at 1000 rpm for 5 min. Then cell mixture was fixed in 4% PFA (Santa Cruz Biotechnology) for 30 min and stored in ice-cold FACS buffer (PBS with 2% FBS (Invitrogen)) at 4 ˚C. The HBMEC and HA fractions in total sample (n=5 for control and n=6 for BLT-1) were obtained by BD FACSAria III Cell Sorter (BD Biosciences, San Jose, CA, USA) and quantitatively analyzed using FlowJo software (FlowJo LLC, Ashland, OR, USA). Debris and doublets were excluded using FSC-A/SSC-A, FSC-A/FSC-W, respectively. The cells were then gated for the appropriate markers for the cell type (Figure S 4.3).

Calculation of nanoparticle distribution on a chip. Loss of the injected NPs in a device due to their non-specific adsorption to the PDMS surface was measured by sampling the

NP solution after 2 h of incubation in a device consisting of a single-layer of the vascular channel. The NP distribution in HBMECs was calculated as follows:

$$(HBMEC\ uptake_{calculation}) = (Total\ injected\ (100\%)_{Sampling}) - (Loss_{sampling}) - (Vascular_{Sampling}) - (Perivascular_{Sampling})$$

Where $(Vascular_{Sampling})$, $(Perivascular_{Sampling})$, and $(Total\ injected\ (100\%)_{Sampling})$ are fluorescence intensities of NP solutions sampled from the vascular channel, perivascular channel, and injected solution, $(Loss_{sampling})$ is the loss of NPs in a device measured by sampling, and $(HBMEC\ uptake_{calculation})$ is percentages calculated by the equation.

4.5 **Supplementary Information**

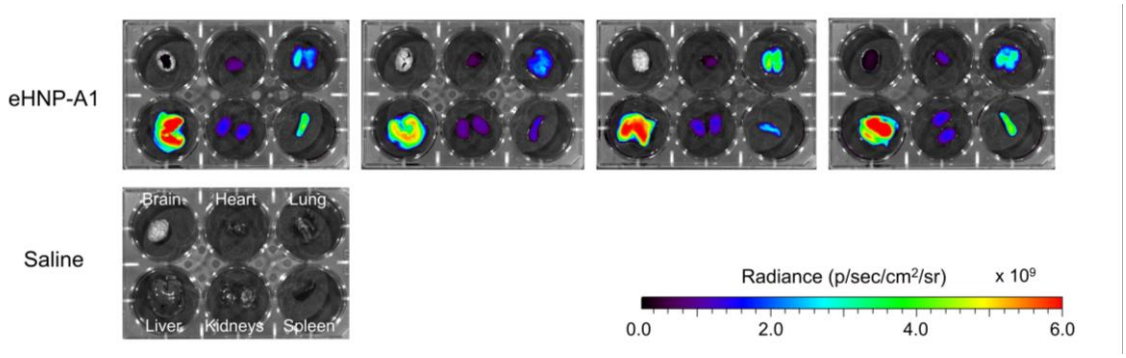

Figure S 4.1 Ex-vivo biodistribution of eHNP-A1. Organ distribution of dye-loaded eHNP-A1 24 h after intravenous administration. Fluorescence signals of eHNP-A1 were detected in the brains as compared to the saline control.

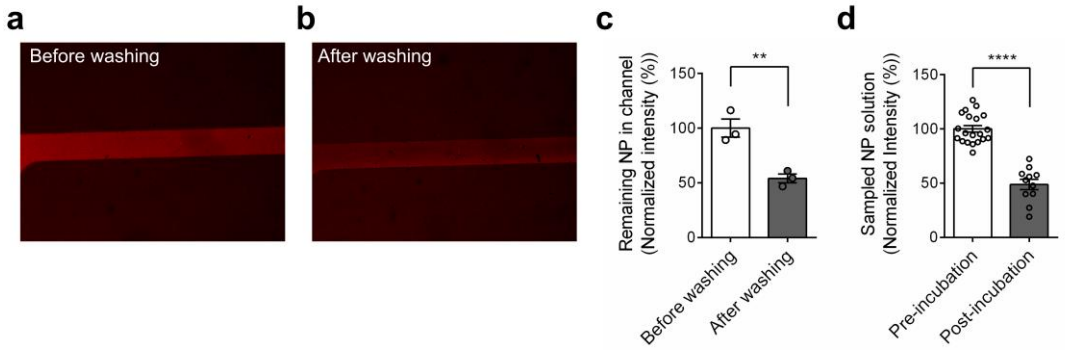

Figure S 4.2 eHNP-A1 loss in a microfluidic channel due to the adsorption to the PDMS surface. a,b, Fluorescent images showing eHNP-A1 solution inside the vascular channel after 2 h of NP incubation before washing the channel (**a**) and after washing the channel with PBS (**b**). Single layer of the vascular channel without cells were used to measure the eHNP-A1 loss caused by adsorption to the PDMS. **c**, Fluorescence intensities in the vascular channel in images quantified using ImageJ, indicating the remaining NPs in the channel. The fluorescence intensities were normalized to that from the channel "before washing" (n=3 for each condition, **p<0.01). **d,** Fluorescence intensities of NP solutions before injecting into the microchannel (pre-incubation) and sampled from the microchannel after 2 h of incubation (post-incubation) measured with a plate reader, indicating working concentration of the NP solution (n=20 for pre-incubation and n=11 for post-incubation, ****p<0.001). The intensities were normalized to those of the pre-incubated NP solution.

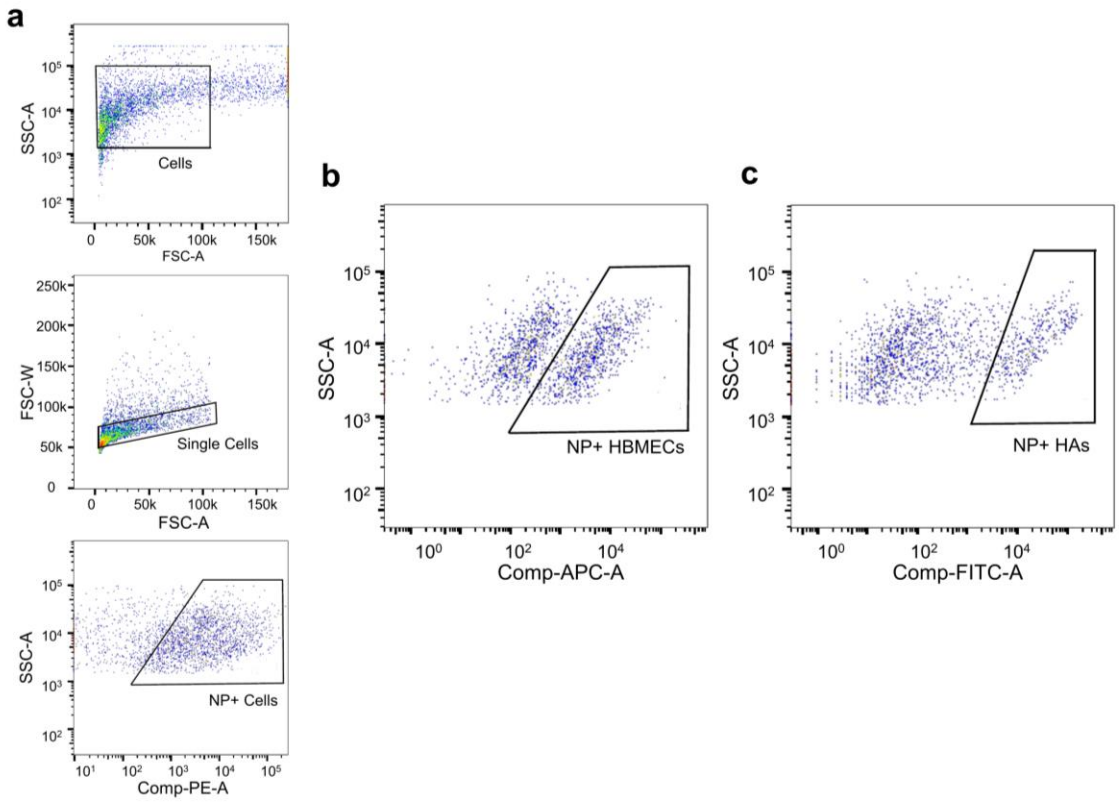

Figure S 4.3 Example of gating strategy for flow cytometric analysis of eHNP-A1$^+$ cells. a, Cell suspensions were hierarchically gated as follows: Cells were gated and debris were excluded using FSC-A/SSC-A. Single cells were selected using FSC-A/FSC-W gate. NP$^+$ cells were distinguished with PE fluorescence. **b,** PE$^+$/APC$^+$ cells were considered as NP$^+$ HBMECs. **c**, PE$^+$/FITC$^+$ cells were considered as NP$^+$ HAs.

CHAPTER 5. CONCLUSIONS

5.1 Concluding Remarks

In this thesis, I have presented a microengineered human BBB platform with physiologically relevant structure and function, offering its application in quantitative assessment of CNS drug delivery systems. The hybrid design of a microfluidic device combining two vertical layers with three parallel channels enabled reconstitution of the BBB structure by establishing a 2D intact brain endothelium and a 3D brain microenvironment with astrocytic network. The *in vivo* like physiology of astrocytes in 3D microenvironment as well as the characteristics of HBMECs with their BBB specific gene expressions in the BBB model were demonstrated. The three human BBB constituent cell types reconstituted the BBB-like structure in a device. Its function was validated with permeability and TEER measurements. Moreover, I for the first time quantified the polarized distribution of AQP4 in the BBB model, which has long been overlooked in existing *in vitro* BBB models. More importantly, the well-designed and validated BBB model precisely captured nanoparticle distributions in the vascular and perivascular regions of the BBB at cellular levels and demonstrated distinct cellular uptakes and BBB penetrations through receptor-mediated transcytosis of high-density lipoprotein-mimetic nanoparticles.

Taken together, the present BBB model has great potential as a complementary *in vitro* model to existing *in vivo* models for predicting drug delivery across the BBB in a mechanistic manner for the treatment of CNS diseases. Thus, this human BBB model could

provide a widely useful tool for translational medicine research in particular for the modeling of neuroinflammation and reactive gliosis in neurological disorders.

5.2 **Challenges and Future Work**

5.2.1 Cell sources

Recent *in vitro* models have demonstrated the importance of cell source to mimic organ-specific function *in vitro*, as well as for human disease modeling.[74,75] In particular, highly complex BBB organization requires brain-specific cells to be sourced appropriately for *in vitro* modeling, which secures the key characteristics including the tight barrier function and low permeability resulting from high expressions of BBB-specific proteins.[5,9,69,70] Immortalized human brain cells are good candidates for standardized screenings due to their availability as well as indefinite proliferation while preserving their properties. Primary human brain cells display functional features that are more relevant to the cells *in vivo*, but their availability is limited with ethical issues and there is another issue with their batch-to-batch variability. Human induced pluripotent stem cells (iPSCs) differentiated into brain cells can provide a robust source that possess properties for human BBB models. Moreover, advances in the iPSC technology can be integrated into the BBB model to develop human BBB models with different genetic backgrounds.

5.2.2 Hydrogel

Among the commercially available hydrogels, Matrigel has the most similar components to the brain extracellular matrix, with laminin and collagen IV as major components. In the BBB model, to minimize the effects of Matrigel on astrocyte reactivity, I have cultured astrocytes in growth-factor reduced Matrigel. Although the cells grow well in Matrigel, there is one issue that can arise when maintaining the culture system for longer-time. Due to its degradation over time, it is hard to maintain the 3D culture over 5 days, which restricts long-term drug screening or disease modelling. Moreover, there are other drawbacks such as Matrigel's tumorigenic origin and batch-to-batch variation. Culturing astrocytes in well-characterized and tunable hydrogels may overcome the challenges in the current Matrigel-based model.

5.2.3 Higher-throughput experimental setup

The current BBB model allowed for multiple analyses including TEER measurement, nanoparticle sampling, and FACS analysis while the multiple devices were regulated by multi-syringe racks at the same time. Microfluidic parallelization technology that integrates multiple devices while preserving advantages of the microscale organ-on-a-chip engineering will further provide higher throughput system.[100]

5.2.4 Reduce the adsorption of molecules in a chip

The present microfluidic device is made of PDMS, which has a critical disadvantage to perform high-precision sampling of biochemical molecules. It has been

reported that PDMS adsorbs many molecules due to its surface properties including porosity and hydrophobicity.[101,102] To reduce the molecular adsorption to channel surface, the PDMS channel can be chemically modified using chemical vapor deposition or silanization.[103] Moreover, a new microfluidic device made of other materials that have less adsorption of molecules, such as polystyrene may solve the molecular adsorption issue.

APPENDIX A.MICROFABRICATION OF THE HUMAN BLOOD-BRAIN BARRIER CHIP

A.1 Overview

This protocol includes the process for the fabrication and functional validation of the microengineered human blood-brain barrier (BBB) chip.

The summary of this protocol is as follows:

Development of the microengineered human BBB chip

a. Fabrication of the chip
b. Cell culture in the chip
c. Flow initiation into a microfluidic channel

Demonstration of the structure and function of the BBB chip

a. Immunofluorescent staining
b. Permeability assay
c. TEER measurement

Figure A 1 Fabrication-completed microengineered devices.

A.2 Development of the microengineered human BBB chip

A.2.1 Chip fabrication

Materials and equipment:

- ✓ PDMS (Sylgard 184 Elastomer Kit)
- ✓ Silicon wafer molds (Upper and Lower channel molds)
- ✓ Polycarbonate membrane – 8 µm pore (Sterlitech PCTB8025100)
- ✓ (3-Aminopropyl)triethoxysilane (APTES) (Sigma 440140) 5% solution in DI water
- ✓ Diamond cutter
- ✓ 1 mm biopsy punch
- ✓ Clear plastic container (Ted Pella 139-75)
- ✓ Kimwipes
- ✓ 100 mm petri dish
- ✓ Scissors
- ✓ Precision knife
- ✓ Tweezers
- ✓ Benchtop microscope
- ✓ Microscope glass slide
- ✓ Scotch magic tape (3M 810) – for cleaning
- ✓ Hot plate
- ✓ Plasma cleaner
- ✓ 80 °C dry oven

Procedure:

1. Mix PDMS pre-polymer (33g for upper channel mold, and 11g for lower channel mold; 10:1 elastomer base to curing agent, wt/wt), degas in vacuum chamber, and pour onto the SU-8 wafers patterned with microchannels.
2. Cure PDMS on the upper channel mold in the 80 ˚C dry oven for 1 hour.
3. Spin PDMS onto the lower channel mold using the following recipe:
    a) Step 1: 100rpm at 50rpm/s for 10 seconds
    b) Step 2: 250rpm at 50rpm/s for 93 seconds
    c) Cure at 100ºC for 5 minutes
4. Cut out the upper PDMS slab and punch inlet/outlet holes using a 1mm biopsy punch (punch into the PDMS from the channel side).
5. Cut out the lower PDMS layer and place lower channel onto a clean glass slide channel side up.
6. Cut and treat polycarbonate membranes for bonding
    a) Heat APTES solution on the 80ºC hot plate for 20 min
    b) Plasma clean the both sides of the membrane for 1 min each
    c) Roughly cut out 3 mm x 10 mm sections of the polycarbonate membrane
    d) Soak the plasma cleaned membrane cutouts into the warmed APTES solution for 20 minutes (While waiting for 20 min, do the steps 7 and 8)
    e) Dry the membrane cutouts on kimwipes
7. Clean the channel side of the upper PDMS slab with tape 3 times.
8. Clean the channel side of the lower PDMS layer with tape 3 times.
9. Assemble PDMS components and membrane together.

a) Plasma clean the lower channel assembly and upper channel.
b) Carefully apply a dried membrane cutout onto the lower channel, making sure to center and cover region where lower and upper channels overlap.
c) Bring lower channel assembly and upper channel to the microscope and bond the two layers together.
    i. Find a cross (+) mark on the lower channel and clamp down the lower channel assembly with the microscope sample clips
    ii. Move the upper channel above the lower channel and focus the microscope lens so that both the upper and lower channels come into focus.
    iii. Carefully align the upper and lower channels so that the crosses in both upper and lower channels are aligned together.
    iv. Gently press the border of the membrane with tweezer.
d) Place the chip in 100 mm petri dish and leave in the 80 °C dry oven for 30 minutes

10. Cut the assembled chip half across the cross mark (The original chip contains two parallel BBB platform).
11. Clean out a plastic box with N2 gas and place the assembled chip in a box to locate the outlet of the upper channel at the right side of the box and the inlets (branched) of the upper channel at the left side of the box.
12. Pour 10 grams of PDMS around the chip to fix the chip in place. Bake in the 80 °C dry oven for 1 hour
13. Mark the outlet on the lid of the box, remove the lid from the box and drill a hole into the lid using 7/64” bit. Reassemble the box with the lid.
14. Sterilize the device with 70% Ethanol.

15. Leave the device in 80°C oven for > 2.5 days before cell culture to allow PDMS surfaces to recover hydrophobicity.

A.2.2 Cell culture

Materials and equipment:

- ✓ Assembled device
- ✓ 70% ethanol
- ✓ PBS 1X
- ✓ Fibronectin (50 µg/mL) (Sigma Aldrich F1141)
- ✓ 1 confluent T75 flask of human brain vascular pericytes (HBVP) (passage 3-5) (Sciencell 1200)
- ✓ 1 confluent T75 flask of human astrocytes (HA) (p3) (Sciencell 1800)
- ✓ 1 confluent T75 flask of immortalized human brain microvascular endothelial cells (HBMEC) (p3-10) (Sciencell 1000)
- ✓ Cell growth media (PM, AM, and ECM) (Sciencell 1201, 1801, 1001)
- ✓ Mixed media for BBB culture (1:1:1 ECM, AM, and MM)
- ✓ Growth factor reduced Matrigel (Corning 354230) – Check the endotoxin level of the lot before ordering
- ✓ 20-200µL pipette and tips
- ✓ Centrifuge

Procedure:

1. Coat the lower side of the membrane with 50 μg/ml of fibronectin (in 1x PBS) for an hour at 37°C).
2. Wash the channel twice with the culture media.
3. Infuse 10 μl of HBVPs (1E7 cells/mL) into the lower channel and flip the whole chip upside down immediately after pinching the inlets and outlets of the lower channel.
4. Add 500 μl of PBS in the plastic box to avoid media drying out.
5. Refresh the cell culture media 1 hour after cell seeding.
6. Culture HBVPs for 6 hours.
7. Inject 10 μl of the astrocytes embedded hydrogel (in the case of Song Ih's BBB, 5 mg/mL of Matrigel) into the lower channel. (HA: 1E6 cells/mL)
8. Flip the chip upside down.
9. Let the hydrogel cure in the incubator (37°C) for 1 hour.
10. Inject the cell culture media in the upper and side channels.
11. Culture HAs for 6 hours.
12. Coat the upper side of the membrane with 50 μg/ml of fibronectin for 1 hour.
13. Wash the upper and side channels twice with the culture media.
14. Infuse 15 μl of HBMECs (7E7 cells/mL) into the upper channel.
15. Refresh the cell culture media in the upper channel 1 hour after cell seeding.
16. Culture the cells for 1 day at 37 °C incubator before applying shear stress into the upper channel.

A.2.2 Flow initiaion

Materials and equipment:

- ✓ PDMS
- ✓ 1-10 µL tips
- ✓ Syringe pump (Harvard apparatus PhD Ultra)
- ✓ Tygon silicon tubing (Cole Parmer 95702-00)
- ✓ PE60 tubing (BD Intramedic 427415)
- ✓ 3mL syringes (BD 309657)
- ✓ 30mL syringes (BD 302832)
- ✓ 18G needles (BD 305180)
- ✓ Clamps

Procedure:

1. Cut the 1-10 µL tips (Fig.1; half of the first line (1) and the first line (2) of the tip) and clog the fine tip with PDMS. Cure PDMS in the tips in 80 °C dry oven for 15 min.

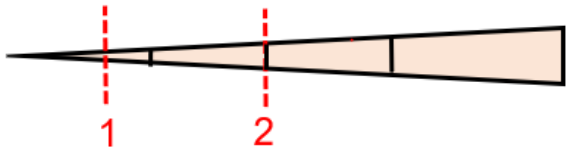

Figure A 2 10 µL tip cutting guideline to make a plug for inlets/outlets.

2. Autoclave the prepared plugs.
3. Close the inlets/outlets of lower channels and branch of the upper channel as shown in Figure A 3.

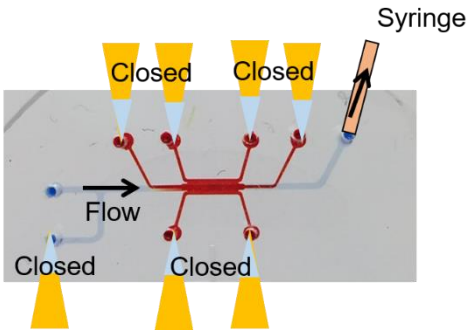

Figure A 3 Closure of the holes of the channels before applying flow into the upper channel.

4. Prepare tubings (detailed description per 1 chip).
    a) 10 cm long tygon tubing
    b) ~50 cm long tygon tubings
    c) 3 mm long PE60 tubing adapters (x2)

* DO NOT autoclave the PE60 tubing adapters. To sterilize, leave the tubing sets under UV overnight.

5. Connect the PE60 tubing with the tygon tubings.
6. Plug the culture medium filled tubing (10 cm long tubing, clamped) in the outlet of the upper channel (PE60 tubing into the outlet) and thread the tubing through the drilled hole in the lid of the plastic box.
7. Add 30 mL of culture media in the plastic box.
8. Place the device in a 37 °C incubator.
9. Prepare a 30 mL syringe filled with 3 mL of culture medium and connect the syringe (18G needle) with a 50 cm long tubing. Fill the entire tubing by pushing the culture medium in the syringe.

10. Set up a syringe pump as described below:
    a) Step 1: (WITHDRAW) Ramp up flow rate from the minimum (0.08 µL for 30 mL syringes) to 16 µL/min for 1 hour
    b) Step 2: (WITHDRAW) Maintain 16 µL/min for 24 hours.
11. Place the tubing connected syringe in a syringe pump and connect the tubings with the tubings connected to outlet of the device.
12. Unclamp the tubes and start the pump run.

A.3 Demonstration of structure and function of the BBB in a chip

A.3.1 Immunofluorescent staining

Materials and equipment:

- ✓ BBB chip
- ✓ Tweezer
- ✓ PBS 1X
- ✓ 2% Paraformaldehyde (PFA)
- ✓ 0.1% Triton-X
- ✓ 2% Bovine serum albumin (BSA)
- ✓ 1% BSA
- ✓ Primary antibodies
- ✓ Secondary antibodies
- ✓ DAPI
- ✓ dH_2O

Procedure:

1. After 24 hrs of flow application, clamp the tubing connected to the outlet of the upper channel and take the device out from the incubator.
2. Remove the plugs and tubing from a chip gently using a tweezer.
3. Wash the upper and side channels with pre-warmed PBS.

- PBS and PFA are pre-warmed to avoid the endothelial cell shrinkage.

4. Add pre-warmed 2% PFA into the upper and side channels and incubate at RT for 15 min.
5. Wash the upper and side channels with PBS for three times.
6. Add 0.1% Triton-X into the upper and side channels and incubate for 15 min at RT.
7. Wash the upper and side channels with PBS for three times.
8. Add 2% BSA into the upper and side channels and incubate for 1 hour at RT.
9. Wash the upper and side channels with PBS for three times.

- After completing this step, the samples can be stored at 4˚C for later use.

10. Add primary antibodies (diluted in 1% BSA to achieve a desired concentration – 3x higher concentration than the recommended concentration) into the upper and side channels and incubate at RT for 3 hours or overnight at 4˚C.
11. Wash the upper and side channels with 1% BSA for five times.
12. Add secondary antibodies (diluted in 1% BSA to achieve a desired concentration – 3x higher concentration than the recommended concentration) into the upper and side channels and incubate for 1 hour at RT or overnight at 4˚C.
13. Wash the upper and side channels with 1% BSA for five times.

14. Add DAPI solution (1:200 in dH_2O) into the upper and side channels and incubate for 5 min at RT.

- DAPI has poor solubility in PBS, but is soluble in water at 20 mg/mL

15. Wash the upper and side channels with dH_2O for three times.

16. Wash the channels with PBS twice.

A.3.2 Permeability assay

Materials and equipment:

- ✓ BBB chip
- ✓ Culture medium (remain in a plastic box after applying flow can be used)
- ✓ Tweezer
- ✓ Clamps
- ✓ Fluorescent probe (e.g. FITC-dextran)
- ✓ Syringe pump (Harvard apparatus PhD Ultra)
- ✓ Tygon silicon tubing (Cole Parmer 95702-00)
- ✓ PE60 tubing (BD Intramedic 427415)
- ✓ 1mL syringes (BD 309657)
- ✓ 30mL syringes (BD 302832)
- ✓ 18G needles (BD 305180)
- ✓ 1.5 mL Eppendorf tube
- ✓ Plate reader

Procedure:

1. After 24 hrs of flow application, clamp the tubing connected to the outlet of the upper channel and take the device out from the incubator.
2. Remove plugs from inlets/outlets of the left side channel and connect culture medium filled tubings (inlet: 10 cm long tubing, outlet: 5 cm long tubing) to inlets&outlets and leave the tubings clamped (Figure A 4).

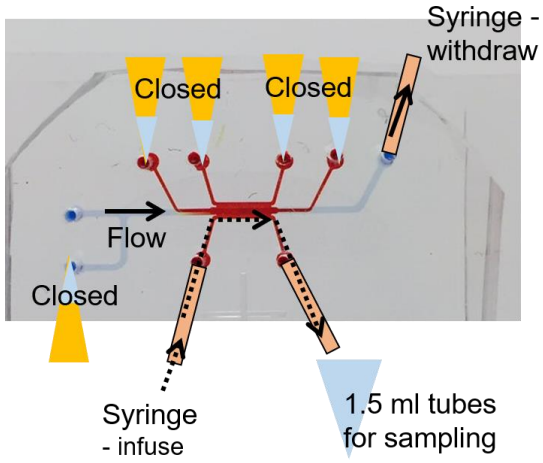

Figure A 4 Tubing and syringe pump setting for permeability assay.

3. Collect the culture medium in a plastic container and add fluorescent probes in the culture medium to make a desired concetration (e.g. present study: 4 kDa and 40 kDa FITC-dextran -500 µg/mL in the cell medium).
4. Add the fluorescent probe added culture medium into a plastic container.
5. Place the device in the incubator, place the side channel outlet tube into a collection tube.
6. Set up two syringe pumps as described below:
    a. Pump 1 (connected to the upper channel): (WITHDRAW) 16 µL/min for 1 hour
    b. Pump 2 (connected to the left side channel): (INFUSE) 4 µL/min for 1 hour.

- The flow rate in both upper and side channels are calculated to achieve 0 pressure differential, to see the diffusion-based permeability.

7. Connect the upper outlet tubing to pump 1 and the side inlet tubing to pump 2.
8. After 1 hour of experiment, read the fluorescence intensities of the collected medium using a plate reader.

- Plain culture medium and fluorescent solutions with known concentrations (1x, 0.5x, 0.25x …) should be measured together to obtain a standard calibration curve.

A.3.3 TEER measurement

Materials and equipment:

- ✓ BBB chip
- ✓ Culture medium (remain in a plastic box after applying flow can be used)
- ✓ Tweezer
- ✓ Sliver wire (A-M systems 783000)
- ✓ Bleach
- ✓ EVOM2 (Word Precision Instruments)

Procedure:

1. Cut the sliver wires with 3 cm length and soak two wires in bleach for 1 hour at RT.
2. Wash the wires with PBS.
3. After 24 hrs of flow application, clamp the tubing connected to the outlet of the upper channel and take the device out from the incubator.

4. Remove plugs from inlets/outlets of the right side channel and connect culture medium filled tubings (3cm long) to inlets&outlets.
5. Connect culture medium filled tubing (3 cm) to inlet of the upper channel as well.
6. Insert the two not bleached silver wires into the tubes connected to the upper channel and the two bleached silver wires into the tubes connected to the right side channel.
7. Connect the other ends of the four tbes to a custom connector to fit EVOM2 voltohmmeter for 4-point measurement.
8. After 1 min of stabilization, read the resistance values 5 times to minimize the reading error.

APPENDIX B. NANOPARTICLE DISTRIBUTION STUDY ON A BBB CHIP

B.1 Overview

This protocol describes the process for use of the microengineered human blood-brain barrier (BBB) chip for studying the nanoparticle distribution.

B.2 Sampling and FACS sample preparation

Materials and equipment:

- ✓ Nanoparticle (NP) solution (fluorophore conjugated)
- ✓ Appropriate fluorophore which is readable in a plate reader should be conjugated.
- ✓ 2~3 fluorescent cell trackers with minimum overlaps of the ex/em wavelengths
- ✓ Fluorophores should not be overlapped with that of NP.
- ✓ Fluorophores should be able to be detected in FACS machine.
- ✓ Dispase 100X
- ✓ 0.25% Trypsin
- ✓ PBS 1X
- ✓ 4% PFA
- ✓ 96-well plate
- ✓ Cell culture media
- ✓ FACS buffer
- ✓ Plate reader

Procedure:

1. Pre-treat cells with fluorescent cell trackers before seeding in a chip.
2. Follow all the steps for cell seeding and flow application described above.
3. Add 10 µL of NP solution (appropriate concentration for NP type (e.g. eHNP-A1: 100 µg/mL) into the upper channel of the chip and incubate for appropriate time (e.g. eHNP-A1: 2 hours).
4. Add a 10 µL drop of culture medium onto the inlet of the upper channel.
5. Withdraw 10 µL of prewarmed PBS from the outlet of the upper channel using 1-20 µL pipette and collect in a 0.6 mL tube.
    a. The collected media is used for measuring the amount of NP solution with a Plate reader.
    b. Add 5 µL of collected solution to 45 µL of culture medium (dilute the collected solution to 0.1x).
    c. Add 5 µL of original NP solution to 45 µL of culture medium.
    d. Place all prepared solutions and 50 µL of culture medium (blank; negative control) in a 96-well and measure the fluorescence intensity of the NPs with a plate reader.
6. Wash the channels with prewarmed PBS once, and add dispase into the lower side channels and trypsin into the upper channel.
7. Incubate the chips in 37 °C incubator for 10 min.
8. Collect all the cells from the upper and lower channels to a 1.5 mL tube.
9. Spin down the collected cells at 1200 rpm for 3 min.
10. Aspirate supernatant and wash the cell pellet with PBS.

11. Spin down the sample at 1200 rpm for 3 min.
12. Aspirate supernatant and add 200 µL of 4% PFA. Incubate for 3 min.
13. Spin down the sample at 1200 rpm for 3 min.
14. Aspirate supernatant, wash with 200 µL of PBS, and spin down. Repeat the step for 3 times.
15. Add 1 mL of FACS buffer (1X PBS + 2% FBS).

REFERENCES

1 Collaborators, G. B. D. N. Global, regional, and national burden of neurological disorders, 1990-2016: a systematic analysis for the Global Burden of Disease Study 2016. *Lancet Neurol* **18**, 459-480, doi:10.1016/S1474-4422(18)30499-X (2019).

2 Mullard, A. Parsing clinical success rates. *Nat Rev Drug Discov* **15**, 447, doi:10.1038/nrd.2016.136 (2016).

3 Daneman, R. & Prat, A. The blood-brain barrier. *Cold Spring Harb Perspect Biol* **7**, a020412, doi:10.1101/cshperspect.a020412 (2015).

4 Zhao, Z., Nelson, A. R., Betsholtz, C. & Zlokovic, B. V. Establishment and Dysfunction of the Blood-Brain Barrier. *Cell* **163**, 1064-1078, doi:10.1016/j.cell.2015.10.067 (2015).

5 Pardridge, W. M. Blood–brain barrier delivery. *Drug Discovery Today* **12**, 54-61, doi:http://dx.doi.org/10.1016/j.drudis.2006.10.013 (2007).

6 Abbott, N. J., Patabendige, A. A., Dolman, D. E., Yusof, S. R. & Begley, D. J. Structure and function of the blood-brain barrier. *Neurobiol Dis* **37**, 13-25, doi:10.1016/j.nbd.2009.07.030 (2010).

7 Calabria, A. R. & Shusta, E. V. A genomic comparison of in vivo and in vitro brain microvascular endothelial cells. *J Cereb Blood Flow Metab* **28**, 135-148, doi:10.1038/sj.jcbfm.9600518 (2008).

8 Soontornmalai, A., Vlaming, M. L. & Fritschy, J. M. Differential, strain-specific cellular and subcellular distribution of multidrug transporters in murine choroid plexus and blood-brain barrier. *Neuroscience* **138**, 159-169, doi:10.1016/j.neuroscience.2005.11.011 (2006).

9 Zlokovic, B. V. The Blood-Brain Barrier in Health and Chronic Neurodegenerative Disorders. *Neuron* **57**, 178-201, doi:http://dx.doi.org/10.1016/j.neuron.2008.01.003 (2008).

10 Armulik, A. *et al.* Pericytes regulate the blood-brain barrier. *Nature* **468**, 557-561, doi:10.1038/nature09522 (2010).

11 Geevarghese, A. & Herman, I. M. Pericyte-endothelial crosstalk: implications and opportunities for advanced cellular therapies. *Transl Res* **163**, 296-306, doi:10.1016/j.trsl.2014.01.011 (2014).

12 Jamieson, J. J., Linville, R. M., Ding, Y. Y., Gerecht, S. & Searson, P. C. Role of iPSC-derived pericytes on barrier function of iPSC-derived brain microvascular endothelial cells in 2D and 3D. *Fluids Barriers CNS* **16**, 15, doi:10.1186/s12987-019-0136-7 (2019).

13 Abbott, N. J., Ronnback, L. & Hansson, E. Astrocyte-endothelial interactions at the blood-brain barrier. *Nat Rev Neurosci* **7**, 41-53, doi:10.1038/nrn1824 (2006).

14 Eidsvaag, V. A., Enger, R., Hansson, H. A., Eide, P. K. & Nagelhus, E. A. Human and mouse cortical astrocytes differ in aquaporin-4 polarization toward microvessels. *Glia* **65**, 964-973, doi:10.1002/glia.23138 (2017).

15 Sofroniew, M. V. & Vinters, H. V. Astrocytes: biology and pathology. *Acta Neuropathol* **119**, 7-35, doi:10.1007/s00401-009-0619-8 (2010).

16 Pekny, M. & Pekna, M. Astrocyte reactivity and reactive astrogliosis: costs and benefits. *Physiol Rev* **94**, 1077-1098, doi:10.1152/physrev.00041.2013 (2014).

17 Almad, A. & Maragakis, N. J. A stocked toolbox for understanding the role of astrocytes in disease. *Nat Rev Neurol* **14**, 351-362, doi:10.1038/s41582-018-0010-2 (2018).

18 Wolburg, H., Noell, S., Wolburg-Buchholz, K., Mack, A. & Fallier-Becker, P. Agrin, aquaporin-4, and astrocyte polarity as an important feature of the blood-brain barrier. *Neuroscientist* **15**, 180-193, doi:10.1177/1073858408329509 (2009).

19 Zamanian, J. L. *et al.* Genomic analysis of reactive astrogliosis. *J Neurosci* **32**, 6391-6410, doi:10.1523/JNEUROSCI.6221-11.2012 (2012).

20 Nagelhus, E. A. & Ottersen, O. P. Physiological roles of aquaporin-4 in brain. *Physiol Rev* **93**, 1543-1562, doi:10.1152/physrev.00011.2013 (2013).

21 Nicchia, G. P. *et al.* The role of aquaporin-4 in the blood-brain barrier development and integrity: studies in animal and cell culture models. *Neuroscience* **129**, 935-945, doi:10.1016/j.neuroscience.2004.07.055 (2004).

22 Saadoun, S. *et al.* Involvement of aquaporin-4 in astroglial cell migration and glial scar formation. *J Cell Sci* **118**, 5691-5698, doi:10.1242/jcs.02680 (2005).

23 Li, L., Zhang, H., Varrin-Doyer, M., Zamvil, S. S. & Verkman, A. S. Proinflammatory role of aquaporin-4 in autoimmune neuroinflammation. *FASEB J* **25**, 1556-1566, doi:10.1096/fj.10-177279 (2011).

24 Esch, E. W., Bahinski, A. & Huh, D. Organs-on-chips at the frontiers of drug discovery. *Nat Rev Drug Discov* **14**, 248-260, doi:10.1038/nrd4539 (2015).

25 Alcendor, D. J. *et al.* Neurovascular unit on a chip: implications for translational applications. *Stem Cell Res Ther* **4 Suppl 1**, S18, doi:10.1186/scrt379 (2013).

26 Kramer, J. A., Sagartz, J. E. & Morris, D. L. The application of discovery toxicology and pathology towards the design of safer pharmaceutical lead candidates. *Nat Rev Drug Discov* **6**, 636-649, doi:10.1038/nrd2378 (2007).

27 Perrin, S. Make mouse studies work. *Nature* **507**, 423-425, doi:DOI 10.1038/507423a (2014).

28 Huh, D. *et al.* Reconstituting organ-level lung functions on a chip. *Science (New York, N.Y.)* **328**, 1662-1668, doi:10.1126/science.1188302 (2010).

29 Cucullo, L., Hossain, M., Puvenna, V., Marchi, N. & Janigro, D. The role of shear stress in Blood-Brain Barrier endothelial physiology. *BMC Neuroscience* **12**, 40-40, doi:10.1186/1471-2202-12-40 (2011).

30 Prabhakarpandian, B. *et al.* SyM-BBB: a microfluidic Blood Brain Barrier model. *Lab Chip* **13**, 1093-1101, doi:10.1039/c2lc41208j (2013).

31 Griep, L. M. *et al.* BBB on chip: microfluidic platform to mechanically and biochemically modulate blood-brain barrier function. *Biomed Microdevices* **15**, 145-150, doi:10.1007/s10544-012-9699-7 (2013).

32 Booth, R. & Kim, H. Characterization of a microfluidic in vitro model of the blood-brain barrier (muBBB). *Lab Chip* **12**, 1784-1792, doi:10.1039/c2lc40094d (2012).

33 Abbott, A. Cell culture: biology's new dimension. *Nature* **424**, 870-872, doi:10.1038/424870a (2003).

34 Watson, P. M. D., Kavanagh, E., Allenby, G. & Vassey, M. Bioengineered 3D Glial Cell Culture Systems and Applications for Neurodegeneration and Neuroinflammation. *SLAS Discov* **22**, 583-601, doi:10.1177/2472555217691450 (2017).

35 Cucullo, L., Hossain, M., Puvenna, V., Marchi, N. & Janigro, D. The role of shear stress in Blood-Brain Barrier endothelial physiology. *BMC Neurosci* **12**, 40, doi:10.1186/1471-2202-12-40 (2011).

36 Reinitz, A., DeStefano, J., Ye, M., Wong, A. D. & Searson, P. C. Human brain microvascular endothelial cells resist elongation due to shear stress. *Microvasc Res* **99**, 8-18, doi:10.1016/j.mvr.2015.02.008 (2015).

37 Siddharthan, V., Kim, Y. V., Liu, S. & Kim, K. S. Human astrocytes/astrocyte-conditioned medium and shear stress enhance the barrier properties of human brain microvascular endothelial cells. *Brain Res* **1147**, 39-50, doi:10.1016/j.brainres.2007.02.029 (2007).

38 Booth, R. & Kim, H. Characterization of a microfluidic in vitro model of the blood-brain barrier (mu BBB). *Lab on a Chip* **12**, 1784-1792, doi:10.1039/c2lc40094d (2012).

39 Cho, H. *et al.* Three-Dimensional Blood-Brain Barrier Model for in vitro Studies of Neurovascular Pathology. *Sci Rep* **5**, 15222, doi:10.1038/srep15222 (2015).

40 Herland, A. *et al.* Distinct Contributions of Astrocytes and Pericytes to Neuroinflammation Identified in a 3D Human Blood-Brain Barrier on a Chip. *PLoS One* **11**, e0150360, doi:10.1371/journal.pone.0150360 (2016).

41 Bang, S. *et al.* A Low Permeability Microfluidic Blood-Brain Barrier Platform with Direct Contact between Perfusable Vascular Network and Astrocytes. *Sci Rep* **7**, 8083, doi:10.1038/s41598-017-07416-0 (2017).

42 Campisi, M. *et al.* 3D self-organized microvascular model of the human blood-brain barrier with endothelial cells, pericytes and astrocytes. *Biomaterials* **180**, 117-129, doi:10.1016/j.biomaterials.2018.07.014 (2018).

43 Park, T. E. *et al.* Hypoxia-enhanced Blood-Brain Barrier Chip recapitulates human barrier function and shuttling of drugs and antibodies. *Nat Commun* **10**, 2621, doi:10.1038/s41467-019-10588-0 (2019).

44 Vatine, G. D. *et al.* Human iPSC-Derived Blood-Brain Barrier Chips Enable Disease Modeling and Personalized Medicine Applications. *Cell Stem Cell* **24**, 995-1005 e1006, doi:10.1016/j.stem.2019.05.011 (2019).

45 Wong, H. L., Wu, X. Y. & Bendayan, R. Nanotechnological advances for the delivery of CNS therapeutics. *Adv Drug Deliv Rev* **64**, 686-700, doi:10.1016/j.addr.2011.10.007 (2012).

46 Masserini, M. Nanoparticles for brain drug delivery. *ISRN Biochem* **2013**, 238428, doi:10.1155/2013/238428 (2013).

47 Kim, J., Ahn, S. I. & Kim, Y. Nanotherapeutics engineered to cross the blood-brain barrier for advanced drug delivery to the central nervous system. *Journal of Industrial and Engineering Chemistry* **73**, 8-18, doi:https://doi.org/10.1016/j.jiec.2019.01.021 (2019).

48 Saraiva, C. *et al.* Nanoparticle-mediated brain drug delivery: Overcoming blood-brain barrier to treat neurodegenerative diseases. *J Control Release* **235**, 34-47, doi:10.1016/j.jconrel.2016.05.044 (2016).

49 Mishra, M. K. *et al.* Dendrimer brain uptake and targeted therapy for brain injury in a large animal model of hypothermic circulatory arrest. *ACS Nano* **8**, 2134-2147, doi:10.1021/nn404872e (2014).

50 Zhang, F. *et al.* Generation-6 hydroxyl PAMAM dendrimers improve CNS penetration from intravenous administration in a large animal brain injury model. *J Control Release* **249**, 173-182, doi:10.1016/j.jconrel.2017.01.032 (2017).

51 Zhou, J. *et al.* Highly penetrative, drug-loaded nanocarriers improve treatment of glioblastoma. *Proc Natl Acad Sci U S A* **110**, 11751-11756, doi:10.1073/pnas.1304504110 (2013).

52 Wang, J. H. *et al.* Dual-Targeting Heparin-Based Nanoparticles that Re-Assemble in Blood for Glioma Therapy through Both Anti-Proliferation and Anti-Angiogenesis. *Advanced Functional Materials* **26**, 7873-7885, doi:10.1002/adfm.201602810 (2016).

53 Sakamoto, A. & Ido, T. Liposome targeting to rat brain: effect of osmotic opening of the blood-brain barrier. *Brain Res* **629**, 171-175 (1993).

54 Huwyler, J., Wu, D. & Pardridge, W. M. Brain drug delivery of small molecules using immunoliposomes. *Proc Natl Acad Sci U S A* **93**, 14164-14169 (1996).

55 Gao, J. Q. *et al.* Glioma targeting and blood-brain barrier penetration by dual-targeting doxorubincin liposomes. *Biomaterials* **34**, 5628-5639, doi:10.1016/j.biomaterials.2013.03.097 (2013).

56 Ahn, S. I., Park, H. J., Yom, J., Kim, T. & Kim, Y. High-density lipoprotein mimetic nanotherapeutics for cardiovascular and neurodegenerative diseases. *Nano Res* **11**, 5130-5143, doi:10.1007/s12274-018-2101-1 (2018).

57 Huang, M. *et al.* GM1-Modified Lipoprotein-like Nanoparticle: Multifunctional Nanoplatform for the Combination Therapy of Alzheimer's Disease. *ACS Nano* **9**, 10801-10816, doi:10.1021/acsnano.5b03124 (2015).

58 Song, Q. *et al.* Biomimetic ApoE-Reconstituted High Density Lipoprotein Nanocarrier for Blood-Brain Barrier Penetration and Amyloid Beta-Targeting Drug Delivery. *Mol Pharm* **13**, 3976-3987, doi:10.1021/acs.molpharmaceut.6b00781 (2016).

59 Robert, J. *et al.* Reconstituted high-density lipoproteins acutely reduce soluble brain Abeta levels in symptomatic APP/PS1 mice. *Biochim Biophys Acta* **1862**, 1027-1036, doi:10.1016/j.bbadis.2015.10.005 (2016).

60 Kuai, R., Li, D., Chen, Y. E., Moon, J. J. & Schwendeman, A. High-Density Lipoproteins: Nature's Multifunctional Nanoparticles. *ACS Nano* **10**, 3015-3041, doi:10.1021/acsnano.5b07522 (2016).

61 Song, Q. *et al.* Lipoprotein-based nanoparticles rescue the memory loss of mice with Alzheimer's disease by accelerating the clearance of amyloid-beta. *ACS Nano* **8**, 2345-2359, doi:10.1021/nn4058215 (2014).

62 Zhang, H. *et al.* Reassembly of native components with donepezil to execute dual-missions in Alzheimer's disease therapy. *J Control Release* **296**, 14-28, doi:10.1016/j.jconrel.2019.01.008 (2019).

63 Aday, S., Cecchelli, R., Hallier-Vanuxeem, D., Dehouck, M. P. & Ferreira, L. Stem Cell-Based Human Blood-Brain Barrier Models for Drug Discovery and Delivery. *Trends Biotechnol* **34**, 382-393, doi:10.1016/j.tibtech.2016.01.001 (2016).

64 Syvanen, S. *et al.* Species differences in blood-brain barrier transport of three positron emission tomography radioligands with emphasis on P-glycoprotein transport. *Drug Metab Dispos* **37**, 635-643, doi:10.1124/dmd.108.024745 (2009).

65 Hajal, C., Campisi, M., Mattu, C., Chiono, V. & Kamm, R. D. In vitro models of molecular and nano-particle transport across the blood-brain barrier. *Biomicrofluidics* **12**, 042213, doi:10.1063/1.5027118 (2018).

66 Sei, Y., Justus, K., LeDuc, P. & Kim, Y. Engineering living systems on chips: from cells to human on chips. *Microfluidics and Nanofluidics* **16**, 907-920, doi:10.1007/s10404-014-1341-y (2014).

67 Placone, A. L. *et al.* Human astrocytes develop physiological morphology and remain quiescent in a novel 3D matrix. *Biomaterials* **42**, 134-143, doi:10.1016/j.biomaterials.2014.11.046 (2015).

68 Sei, Y. J., Ahn, S. I., Virtue, T., Kim, T. & Kim, Y. Detection of frequency-dependent endothelial response to oscillatory shear stress using a microfluidic transcellular monitor. *Sci Rep* **7**, 10019, doi:10.1038/s41598-017-10636-z (2017).

69 Shusta, E. V. Blood-Brain Barrier Genomics, Proteomics, and New Transporter Discovery. *NeuroRx* **2**, 151-161 (2005).

70 Pardridge, W. M. Blood-brain barrier genomics. *Stroke; a journal of cerebral circulation* **38**, 686-690, doi:10.1161/01.str.0000247887.61831.74 (2007).

71 Butt, A. M., Jones, H. C. & Abbott, N. J. Electrical resistance across the blood-brain barrier in anaesthetized rats: a developmental study. *J Physiol* **429**, 47-62 (1990).

72 Wong, A. D. *et al.* The blood-brain barrier: an engineering perspective. *Front Neuroeng* **6**, 7, doi:10.3389/fneng.2013.00007 (2013).

73 Rathore, K. I. *et al.* Lipocalin 2 plays an immunomodulatory role and has detrimental effects after spinal cord injury. *J Neurosci* **31**, 13412-13419, doi:10.1523/JNEUROSCI.0116-11.2011 (2011).

74 Weksler, B. B. *et al.* Blood-brain barrier-specific properties of a human adult brain endothelial cell line. *FASEB J* **19**, 1872-1874, doi:10.1096/fj.04-3458fje (2005).

75 Lee, Y., Ahn, S. I. & Kim, Y. in *Encyclopedia of Biomedical Engineering* (ed Roger Narayan) 384-393 (Elsevier, 2019).

76 Adriani, G., Ma, D., Pavesi, A., Kamm, R. D. & Goh, E. L. A 3D neurovascular microfluidic model consisting of neurons, astrocytes and cerebral endothelial cells as a blood-brain barrier. *Lab Chip* **17**, 448-459, doi:10.1039/c6lc00638h (2017).

77 Man, S. *et al.* Human brain microvascular endothelial cells and umbilical vein endothelial cells differentially facilitate leukocyte recruitment and utilize chemokines for T cell migration. *Clin Dev Immunol* **2008**, 384982, doi:10.1155/2008/384982 (2008).

78 Eigenmann, D. E. *et al.* Comparative study of four immortalized human brain capillary endothelial cell lines, hCMEC/D3, hBMEC, TY10, and BB19, and optimization of culture conditions, for an in vitro blood-brain barrier model for drug permeability studies. *Fluids Barriers CNS* **10**, 33, doi:10.1186/2045-8118-10-33 (2013).

79 Qin, D., Xia, Y. & Whitesides, G. M. Soft lithography for micro- and nanoscale patterning. *Nat Protoc* **5**, 491-502, doi:10.1038/nprot.2009.234 (2010).

80 Aran, K., Sasso, L. A., Kamdar, N. & Zahn, J. D. Irreversible, direct bonding of nanoporous polymer membranes to PDMS or glass microdevices. *Lab Chip* **10**, 548-552, doi:10.1039/b924816a (2010).

81 Young, M. E., Carroad, P. A. & Bell, R. L. Estimation of Diffusion-Coefficients of Proteins. *Biotechnology and Bioengineering* **22**, 947-955, doi:DOI 10.1002/bit.260220504 (1980).

82 Hettiaratchi, M. H. *et al.* A rapid method for determining protein diffusion through hydrogels for regenerative medicine applications. *APL Bioengineering* **2**, 026110, doi:10.1063/1.4999925 (2018).

83 Abbott, N. J. Astrocyte-endothelial interactions and blood-brain barrier permeability. *J Anat* **200**, 629-638 (2002).

84 Alvarez, J. I., Katayama, T. & Prat, A. Glial influence on the blood brain barrier. *Glia* **61**, 1939-1958, doi:10.1002/glia.22575 (2013).

85 Wang, J. D., Khafagy el, S., Khanafer, K., Takayama, S. & ElSayed, M. E. Organization of Endothelial Cells, Pericytes, and Astrocytes into a 3D Microfluidic in Vitro Model of the Blood-Brain Barrier. *Mol Pharm* **13**, 895-906, doi:10.1021/acs.molpharmaceut.5b00805 (2016).

86 DeStefano, J. G., Jamieson, J. J., Linville, R. M. & Searson, P. C. Benchmarking in vitro tissue-engineered blood-brain barrier models. *Fluids Barriers CNS* **15**, 32, doi:10.1186/s12987-018-0117-2 (2018).

87 Yi, Y., Park, J., Lim, J., Lee, C. J. & Lee, S. H. Central Nervous System and its Disease Models on a Chip. *Trends Biotechnol* **33**, 762-776, doi:10.1016/j.tibtech.2015.09.007 (2015).

88 Yuan, W., Lv, Y., Zeng, M. & Fu, B. M. Non-invasive measurement of solute permeability in cerebral microvessels of the rat. *Microvasc Res* **77**, 166-173, doi:10.1016/j.mvr.2008.08.004 (2009).

89 Steiner, J. *et al.* Evidence for a wide extra-astrocytic distribution of S100B in human brain. *BMC Neurosci* **8**, 2, doi:10.1186/1471-2202-8-2 (2007).

90 Jones, V. C., Atkinson-Dell, R., Verkhratsky, A. & Mohamet, L. Aberrant iPSC-derived human astrocytes in Alzheimer's disease. *Cell Death Dis* **8**, e2696, doi:10.1038/cddis.2017.89 (2017).

91 Banks, W. A. From blood-brain barrier to blood-brain interface: new opportunities for CNS drug delivery. *Nat Rev Drug Discov* **15**, 275-292, doi:10.1038/nrd.2015.21 (2016).

92 Vitali, C., Wellington, C. L. & Calabresi, L. HDL and cholesterol handling in the brain. *Cardiovasc Res* **103**, 405-413, doi:10.1093/cvr/cvu148 (2014).

93 Fung, K. Y. *et al.* SR-BI Mediated Transcytosis of HDL in Brain Microvascular Endothelial Cells Is Independent of Caveolin, Clathrin, and PDZK1. *Front Physiol* **8**, 841, doi:10.3389/fphys.2017.00841 (2017).

94 Wang, H. & Eckel, R. H. What are lipoproteins doing in the brain? *Trends Endocrinol Metab* **25**, 8-14, doi:10.1016/j.tem.2013.10.003 (2014).

95 Van Eck, M. *et al.* Differential effects of scavenger receptor BI deficiency on lipid metabolism in cells of the arterial wall and in the liver. *J Biol Chem* **278**, 23699-23705, doi:10.1074/jbc.M211233200 (2003).

96 Kulkarni, A. D., Patel, H. M., Surana, S. J., Belgamwar, V. S. & Pardeshi, C. V. Brain-blood ratio: implications in brain drug delivery. *Expert Opin Drug Deliv* **13**, 85-92, doi:10.1517/17425247.2016.1092519 (2016).

97 Di, L., Rong, H. & Feng, B. Demystifying brain penetration in central nervous system drug discovery. Miniperspective. *J Med Chem* **56**, 2-12, doi:10.1021/jm301297f (2013).

98 Reichel, A. The role of blood-brain barrier studies in the pharmaceutical industry. *Curr Drug Metab* **7**, 183-203 (2006).

99 Sei, Y. J. *et al.* Detecting the functional complexities between high-density lipoprotein mimetics. *Biomaterials* **170**, 58-69, doi:10.1016/j.biomaterials.2018.04.011 (2018).

100 Toth, M. J., Kim, T. & Kim, Y. Robust manufacturing of lipid-polymer nanoparticles through feedback control of parallelized swirling microvortices. *Lab Chip* **17**, 2805-2813, doi:10.1039/c7lc00668c (2017).

101 van Meer, B. J. *et al.* Small molecule absorption by PDMS in the context of drug response bioassays. *Biochem Biophys Res Commun* **482**, 323-328, doi:10.1016/j.bbrc.2016.11.062 (2017).

102 Toepke, M. W. & Beebe, D. J. PDMS absorption of small molecules and consequences in microfluidic applications. *Lab Chip* **6**, 1484-1486, doi:10.1039/b612140c (2006).

103 Zhou, J., Ellis, A. V. & Voelcker, N. H. Recent developments in PDMS surface modification for microfluidic devices. *Electrophoresis* **31**, 2-16, doi:10.1002/elps.200900475 (2010).